



STABILITY OF PROTEIN STABILIZED COCOA BUTTER EMULSIONS UNDER CRYSTALLIZATION

Bachelor thesis for obtaining the academic degree

Bachelor of Science

submitted to the Department 09 - Chemistry, Pharmacy, Geography and Earth Sciences of the Johannes-Gutenberg-University of Mainz



By

Isabel Sabrina Jüngling

born on 22.12.1996 in Munich

30.09.2020

CORE SUBJECT:

First Supervisor:
Second Supervisor:

CHEMISTRY

Prof. Dr. Thomas Vilgis
PD Dr. Wolfgang Schärtl

Table of Contents

Abstract	iii
Kurzfassung	iv
List of Tables	v
List of Figures	vi
List of Abbreviations	ix
<i>General Abbreviations</i>	<i>ix</i>
<i>Formula Symbols</i>	<i>x</i>
1 Introduction	1
2 Theoretical background	2
2.1 <i>Cocoa Butter</i>	2
2.2 <i>Emulsion</i>	5
2.2.1 Emulsifiers	5
2.2.2 Emulsion Preparation	8
2.3 <i>Stability Assessment of Emulsions</i>	10
2.3.1 Crystallization	11
2.4 <i>Rheology</i>	14
2.4.1 Rotational Rheometry	14
2.4.2 Oscillation Rheometry	16
2.4.3 Properties Influencing Rheology of Emulsions	20
3 Material and Methods	22
3.1 <i>Material</i>	22
3.2 <i>Methods</i>	22
3.2.1 Emulsion Preparation	22
3.2.2 Light Microscopy	22
3.2.3 Laser Diffraction Particle Size Analyzer	23
3.2.4 Rheometry	23
3.2.5 Pressure-Test	24
3.2.6 Data Analysis	24
4 Results and Discussion	25
4.1 <i>General Description</i>	25
4.2 <i>Droplet Description</i>	27
4.2.1 Effect of Oil Content	27
4.2.2 Dilution Stability	28
4.2.3 Particle Size Distribution	30

<i>4.4 Crystallization of the Emulsions</i>	34
4.4.1 Crystallization Under Different Circumstances	37
<i>4.5 Behavior of Crystallized Emulsions</i>	41
4.5.1 Network Occurrence	41
4.5.2 Network Stability	42
5 Summary	45
6 Outlook	46
Literature	47
Appendix	51
Acknowledgement	54
Declaration of Originality	55

Abstract

The aim of this research was to investigate the stability of protein stabilized cocoa butter emulsions during crystallization. The surface-active effect of soy protein isolate and its impact on the droplet size distribution of a concentrated cocoa butter emulsion was observed and compared to soy milk, an easily accessible sources of soy protein. As cocoa butter is solid at room temperature, the emulsion was observed during its liquid state, crystallization and crystallized state, through methods such as polarized light microscopy, rotational viscometry, time-dependent oscillatory rheometry, frequency sweep, amplitude sweep as well as pressure tests. The emulsions were prepared with a rotor-stator disperser, the rheological properties were measured with a rheometer. Already established theories for emulsions, such as influence of emulsifier concentration on droplet size, oil content, droplet packing and viscosity, as well as theories for crystalized emulsions on partial coalescence and phase inversion could be applied to the soy protein stabilized cocoa butter system. At the end of the crystallization process no significant difference was observed in the loss factor $\tan \delta$ between the emulsions of different droplet size, describing a viscoelastic solid, which, when pressure or stress was applied, was quite brittle, due to the rigid network formed by cocoa butter crystals.

Kurzfassung

Das Ziel dieser Forschungsarbeit war es, die Stabilität von proteinstabilisierten Kakaobutteremulsionen unter Kristallisation zu untersuchen. Die oberflächenaktive Wirkung von Sojaproteinisolat und sein Einfluss auf die Tropfengrößenverteilung einer konzentrierten Kakaobutteremulsion wurde beobachtet und mit Sojamilch, einer leicht zugänglichen Quelle für Sojaprotein, verglichen. Da Kakaobutter bei Raumtemperatur fest ist, wurde die Emulsion während ihres flüssigen Zustands, der Kristallisation und des kristallisierten Zustandes durch Methoden wie Polarisationslichtmikroskopie, Rotationsviskosimetrie, zeitabhängige oszillatorische Rheometrie, Frequenz-Sweep, Amplituden-Sweep sowie Drucktests beobachtet. Die Emulsion wurde mit einem Rotor-Stator-Dispergierer hergestellt; die rheologischen Eigenschaften wurden mit einem Rheometer gemessen. Bereits etablierte Theorien für Emulsionen, wie Einfluss des Ölgehalts, der Emulgatorkonzentration auf Tropfengröße, die Tropfenpackung und Viskosität, sowie Theorien für kristallisierte Emulsionen über partielle Koaleszenz und Phaseninversion konnten auf das mit Sojaprotein stabilisierte Kakaobuttersystem angewendet werden. Am Ende des Kristallisationsprozesses wurde kein signifikanter Unterschied im Verlustfaktor $\tan \delta$ zwischen den Emulsionen mit unterschiedlicher Tropfengröße beobachtet. Der ermittelte Wert des Verlustfaktor $\tan \delta$ beschreibt einen viskoelastischen Feststoff, der bei Druck- oder Spannungseinwirkung aufgrund des starren Netzwerks, das durch Kakaobutterkristalle gebildet wird, ziemlich spröde ist.

List of Tables

Table 1:Triacylglycerol composition of cacao butter, (compiled from Lipp et al., 2001) analyzing 42 different CBs.	2
Table 2: Melting points in °C of cocoa butter polymorphs determined by different authors. Punctuated in brackets behind the melting points are the used denotation of the respective author. Table taken from (Loisel et al., 1998)	3
Table 3: Interpretation of phase shift δ and $\tan \delta$ (Mezger,2016)	16
Table 4: Settings used for rheological measurements.	24
Table 5: Discription of the droplet size distribution with different values.....	31
Table 6: Determined starting point of curing tcr and crystallization rate, signified through the rise of the storage modulus in time, the gradient m.	39
Table 7: Loss factor $\tan \delta$ at different time points in the crystallization process.	40
Table 8: Yieldpoints γ_L , flowpoints γ_F and flow-transition index γ_L/ γ_F of the different emulsion types.	42

List of Figures

Table of Contents.....	i
Figure 1:P = palmitic acid, O = oleic acid, S = stearic acid, with POS as an example for the structure of a TAG, drawn with ChemDraw Professional	2
Figure 2: (a) subcell structure and (b) chain length structure of TAG crystals. White circles, black circles and zigzag lines mean oxygen atoms, glycerol carbon atoms and hydrocarbon chains, respectively. (Sasaki et. al., 2012)	2
Figure 3: When cacao butter is cooled 'statically' at certain temperatures different crystal forms are adapted and change with time.....	3
Figure 4: Types of emulsions; O = Oil, W = Water, drawn after (McClements, 2010).	5
Figure 5: Arranging of surfactants according to their lipo(tail)- and hydro(head)philic components (modified from McClements, 2010).....	6
Figure 6:Amphoteric headgroup of a protein structure, R symbolizes the sidechain (Müller, 2012).	6
Figure 7:Categorizing of amino acids by charge and polarity (Belitz et al., 2008) , specific amino acid content in used SP see Anhang...(EUROSOY GmbH, 2019).	7
Figure 8: Adsorption of globular and flexible biopolymers, depending on their polar and non-polar segments (McClements, 2010).	7
Figure 9: Through simple shear flow, droplets may experience deformation and rupture, B describing the width and L the length (Walstra,2003).	8
Figure 10: Principle of the Rotor-Stator-System used for homogenization.....	8
Figure 11: Droplet size limiting factor depending on emulsifier regime (McClements, 2010).	9
Figure 12: Depending on the absorption speed of the emulsifier, the droplets produced during homogenization are either stabilized or experience coalescence (McClements, 2010).	9
Figure 13: Dynamical change of surface tension during protein adsorption at the oil-water-boundary (Bergerung et al.,1999)	9
Figure 14: Destabilization of an emulsion through flocculation, coalescence, creaming (sedimentation), breakage or phase inversion.....	10
Figure 15: Free energy changes (ΔG) associated with the solid-liquid phase transition. Below the melting temperature the difference in free energy between the solid and liquid phases (ΔG_{SL}) is negative thereby favoring the solid state, but there may be an activation energy (ΔG^*) associated with nuclei formation that must be overcome before the transition will occur (McClements et al. 2012)	11
Figure 16: Principle of partial coalescence, two partially crystalized droplets meet and merge. This is possible as crystals are now able to grow into a similar surrounding, redrawn after (Walstra, 2003).....	13
Figure 17:Shearing of a sample with rotational movements based on the two-plates model; F = Shear force, v = velocity, A = shear area and h = gap width (Mezger, 2016)	14
Figure 18: Flow curves (left) and viscosity curves (right). 1 = ideally viscous, 2 = shear-thinning, 3 = shear-thickening flow behavior (Mezger, 2016).....	15
Figure 19: Shearing of a sample with oscillatory movements based on the two-plates model with the time-dependant functions of $\tau(t)$, $\gamma(t)$ and $\dot{\gamma}(t)$ in the form of sinus-cosinusoidal curves at ideal elastic behavior; F = Shearforce, s = deflection path, h = plate distance, φ = deflection angle (Mezger, 2016)	16
Figure 20: Amplitude sweep with γ_L as the threshold for the LVE-range. γ_F being the flow point with the sol/gel-transition, on the right side an amplitude sweep with G'' -maximum; modified after Metzger, 2016	18
Figure 21: Time-dependent functions of G' and G'' of a curing process, with the time t_{cr} at the beginning of the phase transition and the time t_{SG} of the sol/gel transition at the intersection point $G' = G''$ (Mezger,2016)	18
Figure 22: Frequency test of two networked polymers. 1 being only slightly connected, 2 a strongly connected polymer (Mezger, 2016).	19
Figure 23: Display of disperse-phase volume fraction (ϕ) systems, ϕ_G = begin glassy systems; ϕ_{RCP} = random close packing, begin crystalline systems; ϕ_{fcc} = face centered cubic packing (McClements, 2010).	20

Figure 24: Solid fat at various length scales (Vilgis, 2015)	21
Figure 25: Phase separation after 30 min because of lacking mechanical energy. Left: CB emulsion prepared with 10 wt% SP; Right: CB emulsion prepared with 1 wt% SP.....	25
Figure 26: Soy protein dispersions with different soy protein content. Upper: 1 wt% SP, Lower: 10 wt% SP	25
Figure 27: Pictures and microscopic images of emulsion before (a) and after (b) emulsification, as well as after crystallization (c) and reheating (d). SP = Soyprotein, CB = cocoa butter	26
Figure 28: Microscope pictures of CB emulsions with $\Phi = 55, 60, 70, 75$ wt% CB content prepared with a 4 wt% SP-dispersion.....	27
Figure 29: Changes of particle size distribution of water diluted CB-SP-emulsions over time.....	28
Figure 30: Creaming of with water diluted emulsion.	28
Figure 31: molecular structure of sodium dodecyl sulfate (SDS).	29
Figure 32: Comparison of different dilution (1:99) compositions; Left: Water; Middle: 1 wt% SDS-Solution + 80 mmol NaCl; Right:1 wt% SDS-Solution + 60 mmol NaCl.	29
Figure 33: Changes of particle size distribution of 1 wt% SDS-solution + 60mmol NaCl diluted 60CB-3SP-emulsions over time.....	30
Figure 34: Microscope pictures of CB-SP-emulsions prepared with left: 3 wt%, middle: 4 wt%, right: 5 wt% - SP dispersions at a magnification of 40x.	30
Figure 35:Droplet size distribution of CB (60 wt%)-emulsions with different SP-concentrations.....	31
Figure 36: Mean and mode diameter of droplets weighted by volume with respect to SP-concentration.	32
Figure 37: Comparison between emulsion prepared with SM, purchased at different times. Left: Emulsion prepared with SM purchased for pre-experiments, middle: Emulsion prepared with SM purchased for experiments, magnification 40x left: Diluted emulsion for experiments, magnification 10x.....	32
Figure 38: Observed flocculation in CB-SP-emulsions. Appearance of "waterstreets".	33
Figure 39: Viscosity curve of CB-SP-emulsions (full symbols) and SP-dispersions (empty symbols).....	33
Figure 40: time-dependent rheological measurement, displaying the storage modulus G' and the loss modulus G'' of a 4SP60CB emulsion complimented by microscope pictures taken seperatly during the same time frame, showing the change in emulsion ofer time. $t_{begin} \approx$ measurement start , $t_p \approx 3000s$, $t_{cr} \approx$ begin of rapid crystallization, $t_{end} \approx$ end of measurement.....	35
Figure 41: Microscope pictures of 4SP60CB-emulsion taken at 100x magnification, red frames: Accumulation of the watery phase. Outside of red frames partial coalescence can be seen.	36
Figure 42: Crystallization at 22°C (upper pictures), followed by a temperature ramp up to 40°C (lower pictures). Effect of partial coalescence on melting behavior.	36
Figure 43:Time-dependent measurement of 3SP60CB measured at 4 °C and 22 °C.	37
Figure 44: Time-dependent measurement of storage modulus of emulsions prepared with different SP-concentrations.	38
Figure 45: Loss factor $\tan \delta$ of time-dependent measurement at different time points in the crystallization process.	40
Figure 46: Frequency sweep of the different emulsion types; left: Storage and loss modulus, right: loss factor $\tan \delta$ at different frequencies.....	41
Figure 47: Amplitude sweep of the different emulsion types; left: Storage and loss modulus, right: loss factor $\tan \delta$ at different γ	42
Figure 48: left: graphical display of pressure experiment, strain = percentage of sample height. right: Random breaking behavior of emulsion samples.	43
Figure 49: Sample after amplitude test.....	43
Figure 51:Time-dependent measurement of emulsions, prepared with different SP-concentrations. Upper plot of two plots of the same color is $\lg G'$, lower $\lg G''$	51
Figure 50: Time-dependent measurement of emulsions, prepared with Soy milk. $\lg G'$ is shown with linear fit to determine t_{cr}	51

Figure 52: Time-dependent measurement of emulsions, prepared with 3 wt% soy protein. $\lg G'$ is shown with linear fit to determine τ_{cr} 52

Figure 53: Time-dependent measurement of emulsions, prepared with 5 wt% soy protein. $\lg G'$ is shown with linear fit to determine τ_{cr} 52

Figure 54: Time-dependent measurement of emulsions, prepared with 4 wt% Soy protein. $\lg G'$ is shown with linear fit to determine τ_{cr} 52

Figure 55: Amplitude-Sweep of emulsions, $\lg G'$ is shown with linear fit. 53

List of Abbreviations

General Abbreviations

CB	Cocoa butter
SP	Soy protein
TAG	Triacylglycerol
P	Palmitic acid
O	Oleic acid
S	Stearic acid
DCL	Double chain length structure
TCL	Triple chain length structure
QCL	Quarto chain length structure
HCL	Hexa chain length structure
(W/O)	Water-in-oil emulsion
(O/W)	Oil-in-water emulsion
HLB	Hydrophilic-lipophilic-balance
SFC	Solid Fat Content
r	Radius
DMA	Dynamic-mechanical analysis
CSR	Controlled shear rate
CSS	Controlled shear strain
wt%	Weight percent
γ_L	Yield point
γ_f	Flow point
(γ_f / γ_L)	Flow transition index
LVE-range	Linear viscoelastic range
t_{cr}	Begin of major crystallization processes
t_{SG}	Sol/gel transition
t_{begin}	Begin of measurement
t_{end}	End of measurement

ϕ	Disperse-phase volume fraction
ϕ_G	Begin disperse-phase volume fraction for glassy systems
ϕ_{RCP}	Begin disperse-phase volume fraction with random close packing
PIDS	Polarization Intensity Differential Scattering
SDS	Sodium dodecyl sulfate
NaCl	Sodium chloride
D	Droplet diameter
$D_{4,3}$	Volume-length mean diameter
D_{mode}	Most common occurring diameter
D_{90}	Diameter of which 90 % of the particles are smaller
D_{50}	Median of particle size distribution
D_{10}	Diameter of which 10 % of the particles are smaller

Formula Symbols

δ	Phase shift
$\tan \delta$	Loss factor
G	Shear modulus
G'	Storage modulus
G''	Loss modulus
γ	Deformation
τ	Shear stress
ω	Angular frequency
h	Parallel-plate distance
A	Surface Area
F	(Shear)-force
$\dot{\gamma}$	Shear rate
v	Velocity
η	Viscosity
s	deflection path

k	Boltzmann-constant
T	Temperature
T_m	Melting Temperature
ΔT_s	Magnitude of supercooling
r_c	Critical radius
γ_i	Solid-liquid interfacial tension
ΔH_{fus}	Enthalpy change of fusion
Δy	Error estimation
$\sigma(y)$	Standard deviation

1 Introduction

Emulsions, although not always visible, play a large role in our daily life. A considerable number of products in our life tend to be emulsions or were at some point of time an emulsion. Especially for food, examples like milk, mayonnaise, butter or ice cream are well known. Although there is a wide variety of physiochemical characteristics among different emulsions, some theories can still be applied to all emulsion-based systems, making food emulsions an interesting subject to study the effects of changed processing or usage of different materials. Understanding emulsions means to apply knowledge from a wide range of different fields of study, such as rheology to gain a better insight on the flow mechanics of emulsions or colloidal science for droplet characteristics. As the interfacial properties also play an important part in the emulsion formation, interfacial chemistry would be another field of study being included to gain an understanding of emulsions. All these fields combined might help to understand the sensory experience, also including sensory sciences and psychology to the related fields. Emulsions and their stability greatly influence this sensory experience and as such it is important to first understand how and when destabilization mechanism occur. Because the stability is influenced by many different factors and studies were performed on different emulsion systems, trying to link microscopic properties and behaviors to the perceived macroscopic ones.

In this thesis, chocolate-soy milk emulsions were chosen as systems under investigation in order to gain a better understanding of the processes and properties occurring when producing an emulsion of a solid fat with a protein solution. If prepared right, these emulsions result in a cr me quite similar to a ganache, displaying a unique texture and mouthfeel. Such organoleptic properties are the result of several processes occurring on microscopic and macroscopic scales, making chocolate-soy milk emulsions a simple yet interesting subject to study. For the preparation of a usual ganache dairy products are used, a chocolate emulsion prepared with soy milk could be an interesting alternative for lactose intolerant person, if dark chocolate is used. As chocolate itself is a complicated system of multiple components, a model system made of cocoa butter, a major ingredient of chocolate, and soy protein was prepared. This facilitates the observation and control of the system, making it possible to associate observed effects to the used material. The behavior of liquid chocolate is already well understood, with the Casson model often used for chocolate rheology. In recent years, although, it was seen that it was restricted to only specific parameters, namely liquid chocolate above 40  C, (Mezger, 2016). Therefore, it would be interesting to study the behavior beneath this temperature.

However cocoa butter-based emulsions are not only used for chocolate products but also for cosmetic and pharmaceutical products. One important aspect is the avoidance of phase separation of the emulsion for at least a certain period. To avoid this, the stability of an emulsion and its dominating destabilization mechanism need to be understood. In order to gain a better understanding, rheology was used to observe changes in stability and was linked to microscopic properties observed under polarized light and to the droplet size distribution.

The next chapter introduces to the theoretical background and will give some insight to the basic theories of emulsions and crystallization in emulsion. In Addition, the effect of crystallization on emulsion stability, as well as to rheological methods used for describing the behavior of a material will be given. Some background information will be given to the material used, as their properties influence the investigated emulsion. The theoretical section is followed by materials and methods. The results of the investigation by methods such as polarized light microscopy, particle size analysis and rheological measurements will be presented in the results and discussion section.

2 Theoretical background

2.1 Cocoa Butter

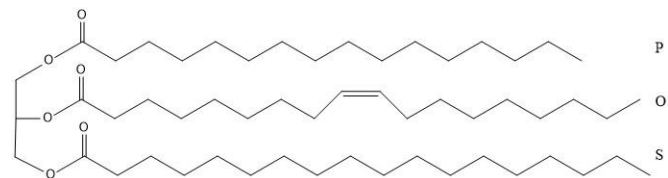
First a short introduction to the main component of the emulsion, the cocoa butter, will be given, as its properties greatly influence the behavior and stability of the emulsion.

Cocoa butter (CB) accounts for approximately 55 % of a cocoa beans weight and can be extracted in presses (Meursing, 1994). As shown in Table 1 below, cocoa butter is mainly composed to approximately 85 % of three triacylglycerols (TAG): POP, SOS and POS. As triacylglycerol is a glycerol esterified with three monocarboxylic acids (fatty acids) (McNaught & Wilkinson, 2009), the three letters symbolize palmitic (P), oleic (O) and stearic (S) acid (Lonchamp & Hartel, 2004), Table 1.

Table 1: Triacylglycerol composition of cacao butter, (compiled from Lipp et al., 2001) analyzing 42 different CBs.

TAG	AVERAGE PERCENTAGE [%]
POP	18.27
SOS	26.39
POS	42.08
OTHER	13.26

Figure 1: P = palmitic acid, O = oleic acid, S = stearic acid, with POS as an example for the structure of a TAG, drawn with ChemDraw Professional



Depending on the composition of TAGs, cocoa butter displays a variety of different melting points and a wide range of polymorphs, influencing the crystals melting and crystallization behavior. (Ghazani & Marangoni, 2019; Sasaki et al., 2012).

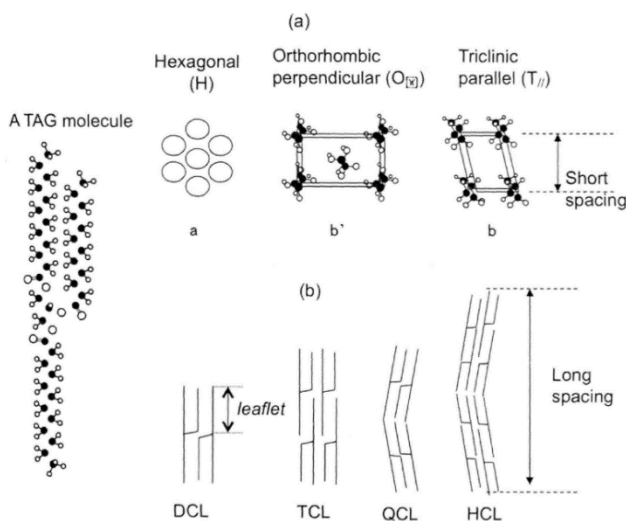


Figure 2: (a) sub cell structure and (b) chain length structure of TAG crystals. White circles, black circles and zigzag lines mean oxygen atoms, glycerol carbon atoms and hydrocarbon chains, respectively. (Sasaki et. al., 2012)

The wide melting range of CB is possible through some high melting TAGs being soluble in lower melting TAGs (McClements, 2012; Walstra, 2003). Six different polymorphs are commonly known and result from different possibilities of highly ordered lateral and longitudinal stacking of the containing TAGs (Loisel et al., 1998). The polymorphs are either denoted with Greek letters to describe their sub cell structure or with roman numbers. The roman numbers are usually ordered in ascending order of the melting points, though some authors are using a descending order. The proper nomenclature often depends on the context and area of interest. Typical polymorph sub cell structures are α (hexagonal), β' (orthorhombic-perpendicular) and β (triclinic-parallel), see Figure 2 a.

In addition, the polymorphs differ in the sequence of the TAGs. These form a chain length structure, which varies from double (DCL) to triple (TCL), quarto (QCL) or hexa (HCL) structures, see Figure 2 b. When the metastable β' -Polymorphs transforms into the thermodynamically stable β -Polymorph, large crystals are formed which changes the rheological properties as well as the taste (Sasaki et al., 2012). In order to avoid this behavior, chocolate is usually tempered with temperature

profiles, to acquire specific polymorphic forms, otherwise, depending on the temperature, different polymorphs of cocoa butter crystals are formed over time, as shown in Figure 3 (Garti & Aserin, 2012; Vilgis, 2015).

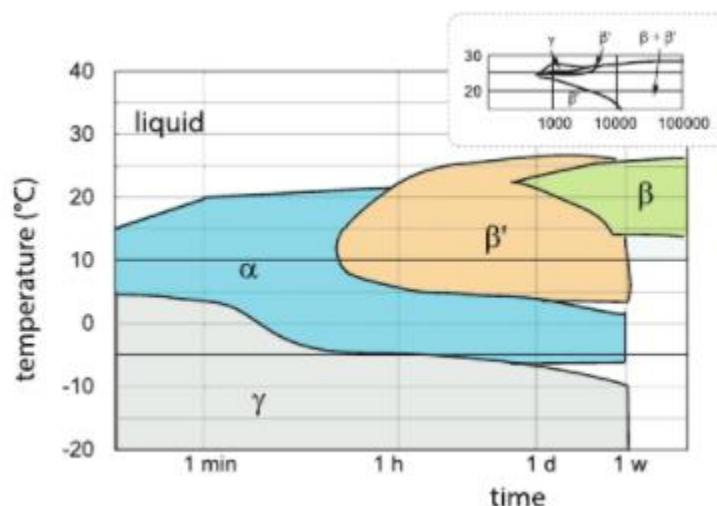


Figure 3: When cacao butter is cooled 'statically' at certain temperatures different crystal forms are adapted and change with time (Vilgis, 2015).

Following Table 2 lists the measured melting points of several authors. As mentioned earlier, they differ notably since the melting point is highly dependent on the composition and ratio of the contained TAGs of the cocoa butter, which itself differs slightly depending on place of origin (Ghazani & Marangoni, 2019; Lipp et al., 2001). It was also found that possible minor components, such as glycolipids, saturated TAGs, phospholipids and other emulsifiers encourage the crystallization, for example through seed nucleation of formed high melt crystals or accelerating as well as retarding polymorph change (Thomas R. Davis & Dimick, 1989; Garti & Aserin, 2012; Loisel et al., 1998). Table 2 also shows quite well the wide range of melting points as well the different notations used in literature.

Table 2: Melting points in °C of cocoa butter polymorphs determined by different authors. Punctuated in brackets behind the melting points are the used denotation of the respective author. Table taken from (Loisel et al., 1998)

References						
(Duck, 1964)	(Wille & Lutton, 1966)	(Chapman et al., 1971)	(Huyghebaert & H. Hendrickx, 1971)(Lovegren et al., 1976)	(Lovegren et al., 1976)	(Merken & Vaeck, 1980)	(T.R. Davis & Dimick, 1986)
°C						
18 (γ)	17.3 (I)		14.9–16.1 (I)	13(VI)	16-18 (γ)	13.1 (I)
23.5 (α)	23.3 (II)		17–23.2 (II)	20 (V)	20.7 (α)	17.7 (II)
	25.5 (III)	20.7 (III)	22.8–27.1(III)	23(IV)		22.4(III)
28 (β'')	27.5 (IV)	25.6 (IV)	25.1–27.4 (IV)	25(III)	26-28 (β')	26.4 (IV)
33 (β')	33.87 (V)	30.8 (V)	31.3–33.2 (V)	30 (II)	33.7–34.9 (β)	30.7 (V)
35 (β)	36.3 (VI)	32.3 (VI)	33.8–36 (VI)	33.5 (I)		33.8 (VI)

Summarized from Table 2, approximately the following melting ranges, denoted with roman numbers in ascending order of the melting point, can be expected: 13–18 °C (I), 17–24 °C (II), 20–28 °C (III), 25–28 °C (IV), 30–35 °C (V) and 32–37 °C (VI).

At room temperature (22°C), polymorph I is still liquid, II and III liquid and/or crystallized and IV, V and VI to be crystallized.

Crystallizing cocoa butter forms a fat crystal network, originating in discrete crystalline particles aggregating to larger microstructures, forming a three-dimensional network. Its mechanical properties are related to the strength and nature of the links between those microstructures. (Joshi et al., 2018; Narine & Marangoni, 1999; Vilgis, 2015).

2.2 Emulsion

An emulsion is a dispersion consisting of two liquid phases, a hydrophilic, aqueous phase (W) and a lipophilic oil phase (O). One phase, the disperse (inner) phase, is distributed in the continuous (outer) phase in the form of droplets. Due to the hydrophobic effect, which prevents the mixing of polar and non-polar molecules, as well as differences in density, these phases, when simply added together, form two clearly separated phases. Emulsions do not form spontaneously, as the direct contact of these two phases is unfavorable both energetically and entropically and therefore, to emulsify these immiscible liquids, sufficient mechanical energy is needed. Although mixed together with high energy, the emulsions are thermodynamically unstable, due to a rise in surface tension. Hence, to avoid the phase separation, the emulsions are kinetically stabilized with the help of emulsifiers. Emulsions are sensitive to temperature changes and often to impact, which can cause the emulsion to separate its phases, thus the emulsion “breaks”.

Due to the large droplet size, emulsions appear to be opaque, often milky, homogeneous mixtures viewed on a macroscopic scale, although when viewed under the microscope the two phases become visible.

The name of the emulsion depends on the dispersion behavior of its phases. If the oil phase is dispersed in the hydrophilic phase, it is referred to as an oil-in-water-(O/W) emulsion and vice versa as a water-in-oil (W/O) emulsion. It is possible for the dispersed phase itself to be an emulsion, in this case the emulsion is referred to as a double-emulsion, see Figure 4. (McClements, 2010).

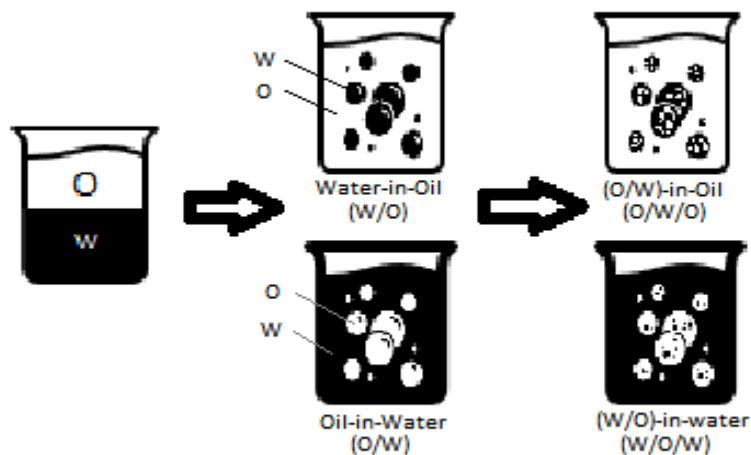


Figure 4: Types of emulsions; O = Oil, W = Water, drawn after (McClements, 2010).

2.2.1 Emulsifiers

As mentioned before emulsions are kinetically stabilized through emulsifiers. The direct contact of the hydro- and lipophilic phases is unfavorable and is prevented by the formation of a boundary layer of amphiphilic, surface-active molecules, called emulsifiers. Well known examples are soap surfactants or in food systems, lecithin. Such small molecule surfactants usually have a hydrophilic headgroup and a lipophilic tail. These molecules find a favorable environmental condition at the phase boundary and arrange themselves according to their lipo- and hydrophilic components, see Figure 5, lowering the contact area, reducing the surface tension. This lowers the free energy of the system through reduction

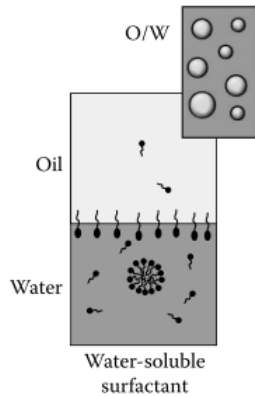


Figure 5: Arranging of surfactants according to their lipo(tail)- and hydro(head)philic components (modified from McClements, 2010).

of the surface energy, which supports further disruption of droplets, enabling mixing. Their concentration also influences the droplet size. In single-phase systems micelles, small spherical aggregates are formed, see Figure 5 . (Gompper et al., 2003; McClements, 2010)

The hydrophilic-lipophilic-balance (HLB) is an important concept to evaluate the affinities of surfactants. The HLB number indicates the ratio of hydro- and lipophilic groups. High HLB numbers (10-18) suggest that the emulsifier is hydrophilic, preferable soluble in water, stabilizing O/W-emulsions. Low HLB numbers (3-6) are lipophilic and preferably soluble in oil, stabilizing W/O-emulsions. In general proteins (the emulsifier used for the researched emulsion) have a fairly high HLB number and are said to be soluble in water, stabilizing oil in water emulsions. (McClements, 2010)

Emulsifiers are categorized by the nature of their hydrophilic headgroup. Ionic emulsifiers, dissolved in water, will dissociate into cations and anions. Depending on the charge of their functional group they are divided between anionic, cationic or, if they have both functional groups, amphoteric surfactants. Depending on the pH-value, the charge of the headgroups will change, changing their emulsification abilities.(Müller, 2012)

2.2.1.1 Soy Proteins as Emulsifier

In this current study soy protein (SP) is used as an example for an emulsifier, as it is an easily accessible, plant-based protein. Soy protein is the protein of the soybean making up approximately 40% or more of the dry matter base (Smith et al., 1996). Soy protein isolate is obtained by de-oiling followed by extracting contained carbohydrates and drying (Belitz et al., 2008; EUROSIOY GmbH, 2019). Soy protein is mainly

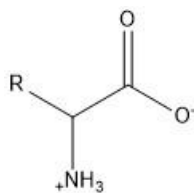


Figure 6:Amphoteric headgroup of a protein structure, R symbolizes the sidechain (Müller, 2012).

composed of four different protein categories distinguished by their sedimentation coefficient:2S, 7S, 11S and 15S (Nishinari et al., 2014). Out of those four 7S and 11S make up most of the proteins contained in SP, the amount depending on the origin of the soy bean (Saio et al., 1969). Soy milk, an easily accessible soy protein source, is produced through grinding of soybeans soaked in water in a ratio of 1:10 (Belitz et al., 2008), containing approximately 3.6 % SP (estimated that soybeans contain around 40+ % SP as mentioned above). Literature reports measured values ranging from 1 – 4% SP in Soy milk (Jiang et al., 2013; Souley & Y, 2009; Zhang et al., 2005).

Soy protein can be considered as pH-dependent ionic emulsifier and contains both anionic and cationic functional groups, classifying it as an amphoteric surfactant. In Figure 6 the amphoteric headgroup of a protein can be seen. (Müller, 2012)

Proteins in general are macromolecules made of different proteinogenic amino acids, connected through peptide bonds (Walstra, 2003). The properties of the protein are determined through the sequence of amino acids, the primary structure of a protein. Amino acids offer different kinds of side changes, influencing the inter- and intramolecular interactions, through their charge and polarity. As such they are categorized into the following, in Figure 7 shown, three groups (Belitz et al., 2008): Non-charged, nonpolar side chains, non-charged, polar side chains and charged side chains, which are further divided into negative charged and positive charged side chains.

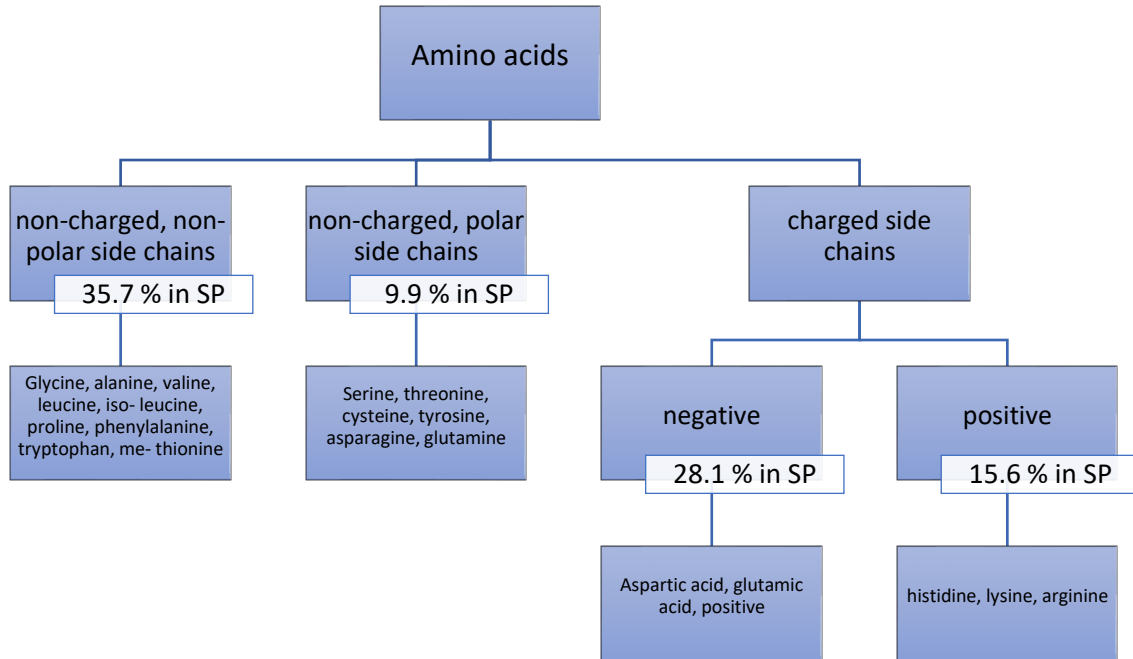


Figure 7: Categorizing of amino acids by charge and polarity (Belitz et al., 2008), specific amino acid content in used SP (EUROSOY GmbH, 2019).

The used SP is mainly consisting of non-charged, non-polar side chains (35.7%), and charged side chains (negative 28.1% and positive 15.6%), as shown in Figure 7. Former preferably interacting with the lipophilic (nonpolar) oil phase and latter interacting with the polar watery phase of the emulsion, same as the polar peptide backbone of the protein, enabling the SP to form an intermediate layer between the phases. The electric charge also enables colloidal solubility through the possible formation of hydrate shells, though it is taunted by adding calcium (Nishinari et al., 2014), a popular supplement in soy milk.

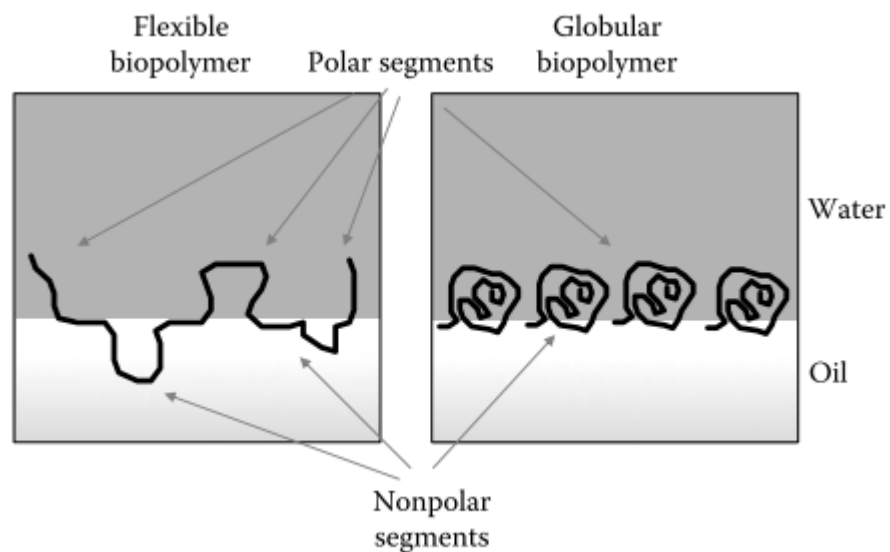


Figure 8: Adsorption of globular and flexible biopolymers, depending on their polar and non-polar segments (McClements, 2010).

During processing the proteins are usually denatured, changing from solely globular to various intermediate unfolded states (Nishinari et al., 2014), which changes the way they are layered around a droplet, see Figure 8. In their globular state, the major amount of segments are unable to freely interact with their preferred surroundings, while in their unfolded state it is easier for the lipo- or hydrophilic parts to arrange themselves according to their preferences and increase their interaction with their preferred surroundings. This also enables a greater surface coverage.

Under heating interactions between SP are possible, enabling gel or film building (Liu et al., 2017). It was found that hydrophobic interactions, as well as hydrogen bonding are important for the network formation (Nagano et al., 1994).

2.2.2 Emulsion Preparation

In the case of the emulsions investigated in this paper, the oil phase is solid at room temperature. As such the fat (cocoa butter) needs to be molten before emulsification. Such emulsions are called melt emulsions. It is a method used to comminute fats, which melt close to room temperature, as those are hard to disintegrate under normal conditions. Another advantage is that precise uniform round shaped particles are acquired instead of oddly and not uniformly shaped particles. Homogenization is performed with either ultra-sound processors, membranes or rotor-stator systems (Müller, 2012). In this thesis a rotor-stator-system was chosen for emulsion preparation. In Figure 10 such a rotor-stator-system is shown. The rotor rotates, while the stator remains static, introducing a shear flow to the sample with a prechosen rotation number per minute (rpm), which influences the produced droplet size. The medium to be processed is automatically drawn axially into the dispersing head through the rotation and then pressed radially through the slots of the rotor-stator arrangement. In between the rotor and the stator the medium experiences simple shear flow, first deforming, then breaking up the droplets into smaller ones, if the surface energy gets too large due to the deformation and enough shear energy is applied to cause smaller droplets as it lowers the through shear experienced deformation, see Figure 9. (IKA® WERKE, 2006; Walstra, 2003)

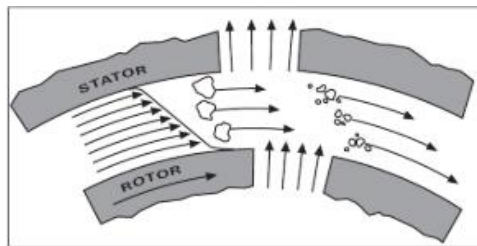


Figure 10: Principle of the Rotor-Stator-System used for homogenization.

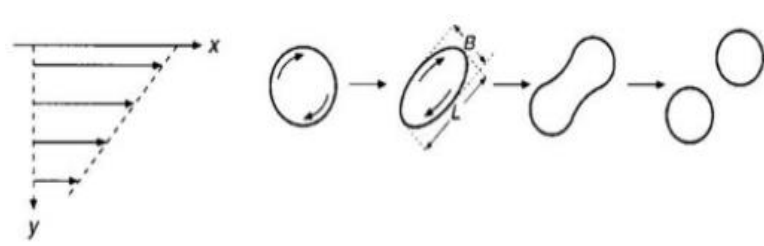


Figure 9: Through simple shear flow, droplets may experience deformation and rupture, B describing the width and L the length (Walstra, 2003).

As mentioned before the droplet size depends on one hand on the initial set speed as it determines the primary droplet size and on the other hand on the amount of emulsifier present. As seen in Figure 11 the limiting droplet size factor is either the emulsifier in emulsifier-poor regimes or the homogenizer in emulsifier-rich regimes. But it also depends on the absorption speed of the emulsifier lowering the surface energy and forming protective layers, as it prevents coalescence, the merging of smaller droplets to larger droplets, as seen in Figure 12. (McClements, 2010; Walstra, 2003).

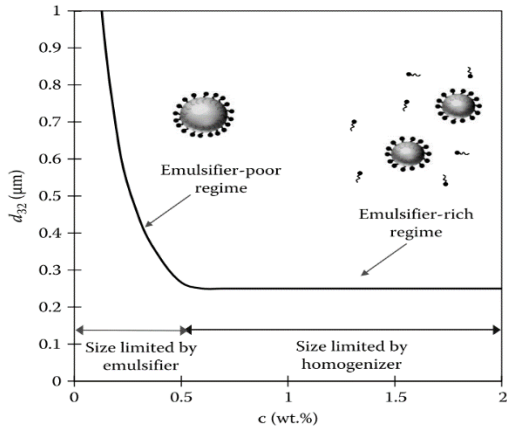


Figure 11: Droplet size limiting factor depending on emulsifier regime (McClements, 2010).

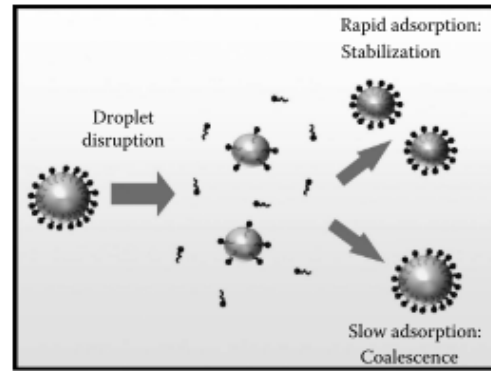


Figure 12: Depending on the adsorption speed of the emulsifier, the droplets produced during homogenization are either stabilized or experience coalescence (McClements, 2010).

Proteins are not adsorbed at once at the boundary. The lowering of the surface tension through protein adsorption can be separated in three phases, as shown in Figure 13:

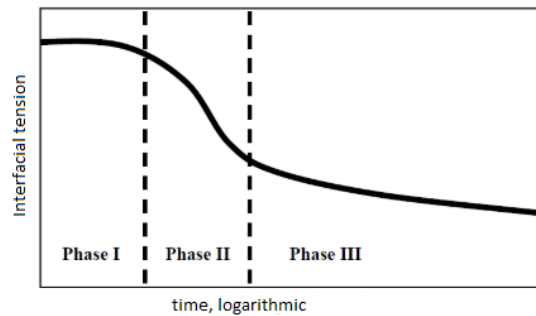


Figure 13: Dynamical change of surface tension during protein adsorption at the oil-water-boundary (Beverung et al., 1999)

Phase I is the induction phase, with only slight lowering of the surface tension. In this phase proteins diffuse from their solvent medium to the boundary, followed by phase II, when the proteins become adsorbed. They are forming a layer reaching an energetically favorable state. In Phase III the surface tension does not decrease much anymore, as it is dominated by arranging the proteins in the best possible way. (Beverung et al., 1999)

It might even be preferable to arrange the proteins in multiple layers, although this depends on the kind of protein used, their concentration, charge and their interactions with each other. The adsorption rate influences the possible droplet size achieved during homogenization (McClements, 2010). It was found that the adsorption of protein on droplet surface is influenced by the solid fat content (SFC) in the droplets (Sugimoto et al., 2001), as they might adsorb to the formed nuclei, inhibiting further growth of the crystals. (McClements, 2010)

2.3 Stability Assessment of Emulsions

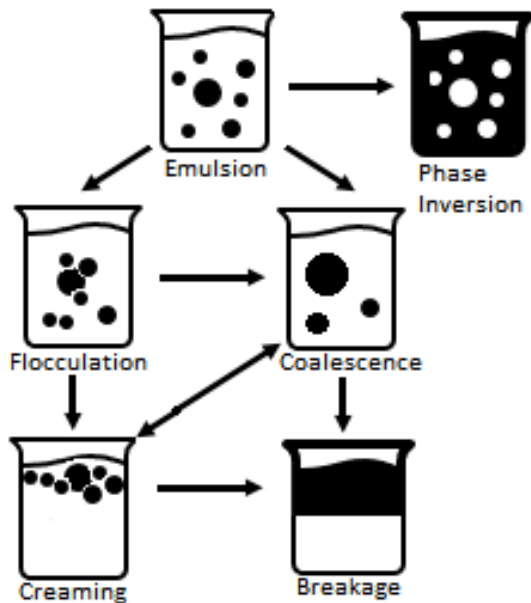


Figure 14: Destabilization of an emulsion through flocculation, coalescence, creaming (sedimentation), breakage or phase inversion.

The slower physical or chemical changes occur, the more stable an emulsion is. For a stability analysis, these changes in properties are considered and investigated (McClements, 2010). Emulsion stability is also often defined through the velocity at which the phases are separating (Pearce & Kinsella, 1978), as this is the main focus when, e.g. a consumer, is looking at a product.

Emulsions are only stabilized through emulsifiers and as such the interactions of the emulsifiers with its surroundings plays an important role in stabilizing an emulsion. An emulsifier influenced destabilization mechanism (all destabilizing mechanism see Figure 14) is flocculation. Flocculation occurs if droplets, through attractive interactions of the emulsifier layers, are grouping together without merging. Stability derives from the ability of the surfactant to produce repulsive interactions, either electrostatically or sterically to keep droplets apart. Flocculation supports the occurrence of coalescence where smaller droplets merge to form larger

droplets, which reduce the overall surface area resulting in an overall reduction of free energy. Another destabilization occurs through gravitational force, as the mixed oil and water are usually of different densities leading to creaming or sedimentation (further on, if referred to creaming, sedimentation can be applied as well, depending on the density of involved parts). Its occurrence is supported by and supports flocculation or coalescence, as the droplets are in proximity for an extended period. Its occurrence is also supported by those two destabilization mechanism as larger droplets cream faster than smaller droplets, as well as diluted emulsions compared to concentrate ones, as flocculation increases, creating three-dimensional networks confining the droplets, hindering single droplet movements. The three-dimensional network can further be strengthened through crystallization, creating a crystal network, which creation can also be influenced through the emulsions shear history and crystal-morphology and composition. Another point concerning crystallization is, that the density of solid fat ($\rho \approx 1200 \text{ kg m}^{-3}$) is higher than that of liquid fat ($\rho \approx 910 \text{ kg m}^{-3}$) (McClements, 2010). An oil droplet has approximately the same density as water if it contains around 30 % solid fat. Changes of the solid fat content (SFC), through nucleation or temperature changes, might change the long-term stability of an emulsion. Increase of the viscosity of the continuous phase, also prevents creaming as it decreases the velocity of the dispersed droplets. The consequence of destabilization is a phase separation, the so-called breakage of the emulsion. Emulsifiers inhibit the separation process and stabilize the emulsion. The amount needed depends on the total surface area of the droplets, the coverage ability of the surfactant and the binding affinity for the interface. (McClements, 2010)

A phase inversion occurs if a W/O- emulsion transforms into an O/W-emulsion and vice versa. Emulsions are capable of phase inversion if they are kinetically stable before and after the transformation. It can be differed between two types of phase inversions: surfactant- and fat crystallization-induced phase

inversion. Surfactant-induced phase inversion occurs in emulsions stabilized with small molecule surfactants and origins in the change of surrounding conditions, favoring different molecular arrangements. Protein stabilized emulsions usually do not display this kind of phase inversion as for one they are more likely to stabilizing O/W-emulsions, due to their high HLB-Value and second they are quite large and less influenced by for example dehydration of the headgroup, as it is mainly dominated by the properties of its sidechains. Fat crystallization-induced phase inversion is based on partial coalescence (chapter 2.3.1.2) forming a continuous fat crystal network trapping water droplets under shearing. Butter and chocolate are emulsions prepared through fat crystallization-induced phase inversion. (McClements, 2010)

As the rheology of a system is determined by its continuous phase, a phase inversion will be displayed by a change of viscosity (Allouche et al., 2004). In this current study, fat crystallization induced phase inversion is assumed to be possible to be observed, with the liquid cacao butter crystallizing in the emulsion.

2.3.1 Crystallization

As cocoa butter is solid under ambient conditions, and the emulsion is prepared from the molten cocoa butter, following chapters will discuss the reason behind crystallization and its effect on emulsions.

For crystallization to occur a nucleus is needed. A nucleus can be formed, when the temperature is below

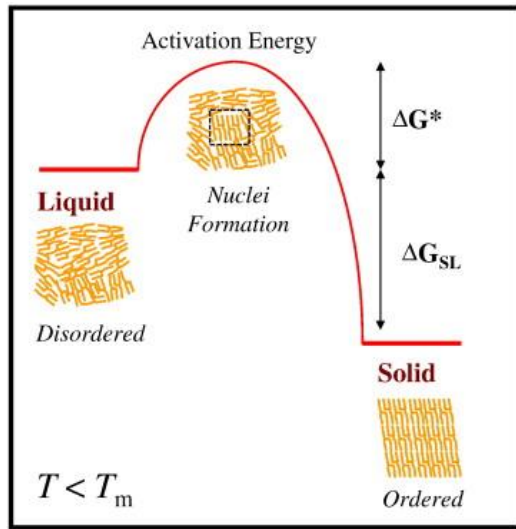


Figure 15: Free energy changes (ΔG) associated with the solid-liquid phase transition. Below the melting temperature the difference in free energy between the solid and liquid phases (ΔG_{SL}) is negative thereby favoring the solid state, but there may be an activation energy (ΔG^*) associated with nuclei formation that must be overcome before the transition will occur (McClements et al. 2012)

the melting point of the substance, as the difference of the free energies between the liquid and the solid state will be negative, favoring the solid state. In many cases, even though the temperature condition is achieved, nucleus formation will not take place immediately. As the nucleus formation requires energy, an activation barrier needs to be passed (Figure 15). As long as the activation energy is higher than the thermal energy (kT , k is the Boltzmann constant) of the system, a supercooled liquid in a metastable state exists. The magnitude of supercooling ΔT_s is defined as the difference between melting temperature and actual temperature of the system

$$\Delta T_s = T_m - T \quad (1)$$

with T_m being the melting point and T the temperature (McClements, 2010).

A stable nucleus is needed for further crystal growth. Nuclei are spontaneously formed through ordered association of molecules. As the formation of a nucleus changes the free energy of the system, a critical radius r_c can be determined. For radii r smaller than r_c a nucleus is unstable and dissolves. Is it larger, a stable nucleus is formed and crystal growth

occurs. The following equation describes the relation between r_c and magnitude of supercooling:

$$r_c = \frac{2\gamma_i T_m}{\Delta H_{fus} \Delta T} \quad (2)$$

With γ_i describing the solid-liquid interfacial tension, being proportional to the unfavorable, positive free energy change of the free energy needed to be input to overcome the new interfacial tension between the liquid and solid state. ΔH_{fus} describes the (negative) enthalpy change of fusion per unit volume associated with the liquid–solid transition, being proportional to the favorable, negative free energy change. The equation shows that with a higher magnitude of supercooling, the critical radius required to form a stable nucleus decreases. Stable nuclei are thus formed more easily at lower temperatures, although a maximum is usually observed, deviating from the equations prediction, because increasing viscosity hinders further diffusion of molecules. (McClements, 2010)

2.3.1.1 Crystallization in Emulsion

The crystallization in emulsions cannot be equivalent to bulk crystallization, because of the geometrical confinement of the oil in droplets. Thus, the physical processes need to follow partially different rules. Crystallization in emulsions occurs, with each droplet showing individual crystallization behavior (Abramov et al., 2016). Large droplets on the one hand have a tendency to crystallize near to the bulk crystallization temperature, as their properties are more similar. More available molecules and a higher degree of movement freedom in larger droplets favor nuclei formation. Small droplets on the other hand can experience large supercooling before they crystallize. (McClements, 2012)

The following distinction can also be made for crystallization in bulk material, but the following description will concentrate on crystallization in emulsion. Homogenous and heterogeneous nucleation need different considerations. The former describes nucleation in the pure oil e.g. in the middle of an emulsion droplet, the latter takes place through contact with foreign surfaces and is further divided into primary and secondary types. Primary heterogeneous nucleation occurs through foreign surfaces with different chemical structures, such as dust particles or reverse micelles of the emulsifier. Secondary heterogeneous nucleation occurs through foreign substances of similar chemical structure in close vicinity. (Fredrick et al., 2010; Walstra, 2003) Those substances can cause, depending on their origin, two different kinds of crystallization processes in emulsions. A primary crystallization process is initiated by seed crystals remaining in the previously heated oil, a secondary crystallization process is initiated through fat crystals of the oil penetrating through collision from a partially crystallized droplet into another one, causing them to stick together, which leads to partial coalescence (Fredrick et al., 2010; Hindle et al., 2000).

2.3.1.2 Partial Coalescence

The phenomenon of fat crystals penetrating from one droplet into another droplet, creating 'bridges', causing them to stick together is called partial coalescence and happens through collision, see Figure 16. A key requirement for partial coalescence are the partial crystallized and partial liquid droplets in supercooled substances, as a solid fat crystal needs to penetrate into the liquid oil phase, so that it remains in chemical similar surroundings, through the liquid oil enveloping it. If the droplets were either liquid or solid, other mechanisms, such as coalescence or segregation would take place. (Fredrick et al., 2010; McClements, 2010).

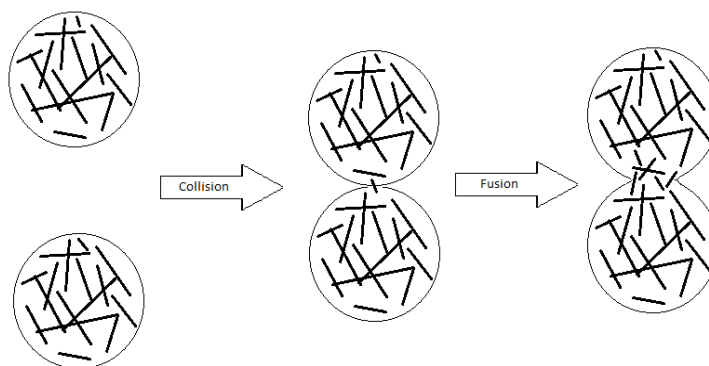


Figure 16: Principle of partial coalescence, two partially crystallized droplets meet and merge. This is possible as crystals are now able to grow into a similar surrounding, redrawn after (Walstra, 2003)

Partial coalescence accounts for the observation of droplets in close proximity of already crystallized droplets crystallizing next, without completely merging (Abramov et al., 2016). Through partial coalescence an emulsion will experience a rapid increase of viscosity and sometimes even phase-inversion if an extensive fat network is formed (McClements, 2010). Due to the mechanical strength of the fat network, the aggregates thus formed retain, at least partially, their droplet shape (Fredrick et al., 2010). At a fat-specific solid fat content (SFC) the rate of partial coalescence is at its maximum. With further increase the rate slows down until everything is crystallized (Fredrick et al., 2010). Another factor influencing partial coalescence is the emulsifier as the layer surrounding the droplet, which either protects from or promote further contact with other, already partially crystallized, droplets, depending on repulsive or attractive interactions of the emulsifier. Proteins form a thicker layer than small molecule surfactants, further inhibiting crystal growth into the neighboring droplet. Another protection from partial coalescence is the repulsive interaction between the polar and non-polar phases because fat crystals will not be able to grow outside their non-polar surroundings. Closed (concentrated) packing of an emulsion instead of diluted ones, or flocculation also promote partial coalescence, because the contact time of similar phase compositions will be increased. Shear also promotes partial coalescence, as it increases the collision frequency as well as efficiency (droplets are closer and impact allows for easier penetration), also influencing possible crystal shape and size. (McClements, 2010)

Partial coalescence contributes to extensive coalescence upon heating such an emulsion (phase transition to solely liquid), increasing for example the mean droplet size or assist further inversion of the emulsion (Thanasukarn et al., 2004, 2006).

2.4 Rheology

Rheology is the study of the flow and deformation of matter. Samples that are analyzed range from ideal viscous liquids to ideal elastic solids. Ideal viscous liquids are described by the law of viscosity, visualized through a damper model. All energy put into these kinds of systems is lost and the material is permanently deformed. Ideal elastic solids on the other hand are described by the law of Hooke, visualized through a spring model. All energy put into these systems is stored and released again if the (3) deformation process ends. The material will return to its original state. Materials are often a combination of those two states. They are described as plastic or viscoelastic materials. Plastic materials behave similarly to a solid beneath a certain yield stress and like a fluid above it. Viscoelastic materials display both properties simultaneously. Examples for such materials are butter or crèmes.

Two popular methods performed to investigate the behavior of a substance are either rotational test or oscillation test. Rotational rheology is used to investigate the flow behavior of a viscous material. Oscillation measurements enables the measurement of a varied range of viscoelastic materials. It is also called dynamic-mechanical analysis (DMA). A model generally used to define the basic rheological parameters is the two-parallel plates model, see Figure 17. A sample is sheared while in between two plates with a gap distance h . The upper plate with a surface area A is moved with a shear force F , resulting in a velocity v . It moves either with oscillating or with rotating movements, depending on the rheometry type performed, while the lower plate remains static ($v = 0$).

Following is the definition of the rheological parameter shear stress τ , used for rotational as well as oscillation tests: (Mezger, 2016)

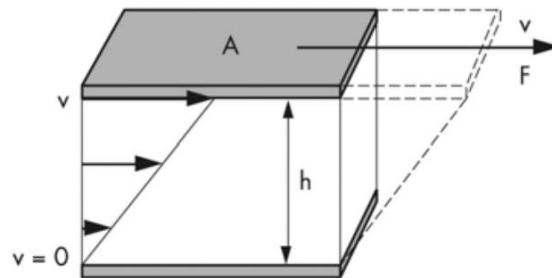


Figure 17: Shearing of a sample with rotational movements based on the two-plates model; F = Shear force, v = velocity, A = shear area and h = gap width (Mezger, 2016)

$$\tau = \frac{F}{A}$$

The following conditions need to be met to allow for exactly defined parameters: The sample is not allowed to slip and the sample needs to deform as homogenously as possible.

2.4.1 Rotational Rheometry

Rotational tests are used to measure the flow behavior of a sample. As the upper plate is rotating, the velocity v is often denoted with the angular frequency ω . The resulting shear rate $\dot{\gamma}$ is defined by the ratio of the speed v to the plate distance h :

$$\dot{\gamma} = \frac{v}{h} \quad (4)$$

Following the law of Viscosity, the viscosity η can be derived from the shear rate and the shear stress. Following equation describes the viscosity η :

$$\eta = \frac{\tau}{\dot{\gamma}} \quad (5)$$

Experiments can be either performed with preset shear rate or preset shear strain. Controlled shear rate (CSR) experiments simulate processes depending on the flow velocity, for example the flow through a tube. Controlled shear stress (CSS) experiments simulate process depending on force, for example squeezing a paste out of a tube. Either way the preset parameter is, during the measurement, either raised or decreased stepwise. For calculating the viscosity, the operation mode is irrelevant.

For evaluating the flow behavior two different graph representations are possible. Either the shear strain versus the shear rate as a flow curve Figure 18 (left) or the viscosity versus the shear rate as a viscosity curve Figure 18 (right). This can be done independently of the operation modes.

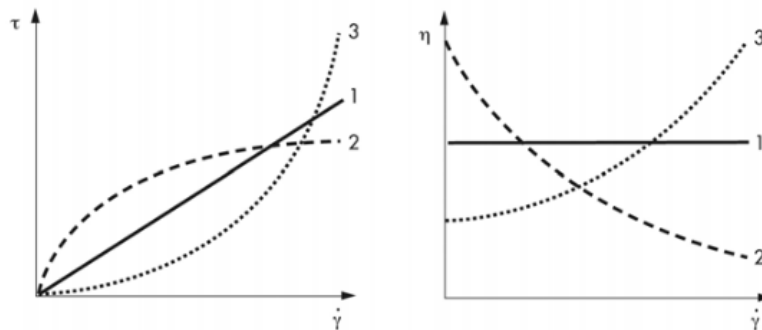


Figure 18: Flow curves (left) and viscosity curves (right). 1 = ideally viscous, 2 = shear-thinning, 3 = shear-thickening flow behavior (Mezger, 2016).

For ideal viscous liquids, the viscosity is independent of the shear rate and would display a linear curve progression, as seen in Figure 18 for graph 1. A curve progression typical for shear-thinning behavior is displayed by Graph 2 of Figure 18. The viscosity of a system decreases as the shear rate increases. This is typical for emulsions because the spherical droplets are deformed to ellipsoids, which are arranged in flow direction, enabling easier flow, as shown in Figure 9. Another possible behavior observed is shear-thickening. In this case the viscosity rises as the shear rate increases, as seen with Graph 3 from Figure 18 (right). This is observed for dispersions of high particle concentrations with either solid or gel-like particles. Through the rotation of the plates, the particles themselves also rotate. Depending on their shape, especially if they are not spherical, they might need more space for rotating, than in their resting state. The viscosity increases. Shear-thickening can also sometimes be observed for emulsions. Through the applied shear, the average droplet size might lower as droplets are divided. The volume-specific surface rises, the interaction between the droplets increases, increasing the flow resistance.

Pure cocoa butter shows the behavior of a Newtonian fluid at temperatures above 30°C and non-Newtonian behavior at temperatures below. The reason for this is the appearance of crystals through the lower temperature being in the melting point range of cocoa butter (Landfeld et al., 2000).

2.4.2 Oscillation Rheometry

Oscillatory tests are used to measure viscoelastic behavior. As mentioned before, the two-plates model is used to explain the oscillatory test. The upper plate is moved by a shaft mounted to driving wheel, resulting in a back and forth motion parallel to the lower plate. The sample is sheared through the oscillatory movements, which remain constant if the rotational speed remains constant. This results in a

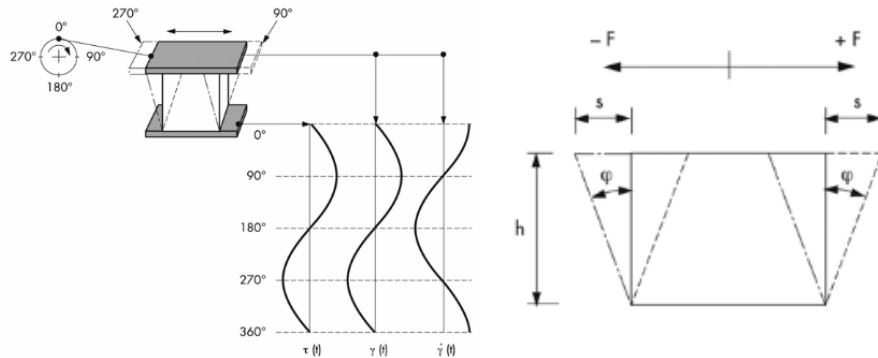


Figure 19: Shearing of a sample with oscillatory movements based on the two-plates model with the time-dependent functions of $\tau(t)$, $\gamma(t)$ and $\dot{\gamma}(t)$ in the form of sinus-cosinusoidal curves at ideal elastic behavior; F = Shear force, s = deflection path, h = plate distance, ϕ = deflection angle (Mezger, 2016)

shear strain (or deformation) γ , describing the ratio of deflection path s of the upper plate and the distance between the two plates h :

$$\gamma(t) = \frac{s(t)}{h} \quad (6)$$

Both the shear strain γ , as well as the shear stress τ result, through the oscillatory movements, in time dependent sinusoidal curves, see Figure 19. The displacement or phase shift δ between those two sinusoidal curves describes the viscoelastic behavior of the sample as shown in Table 3. The phase shift is always between 0° and 90° . At $\delta = 0^\circ$ ideally elastic deformation behavior prevails and at $\delta = 90^\circ$, ideal viscous flow behavior.

Table 3: Interpretation of phase shift δ and $\tan \delta$ (Mezger, 2016)

Liquid		solid			
Ideal behavior	viscous	Behavior of a viscoelastic fluid	Viscoelastic behavior with equally large viscous and elastic components	Behavior of a viscoelastic gel or solid	Ideal elastic deformation behavior
$\delta = 90^\circ$		$90^\circ > \delta > 45^\circ$	$\delta = 45^\circ$	$45^\circ > \delta > 0^\circ$	$\delta = 0^\circ$
$\tan \delta \rightarrow \infty$		$\tan \delta > 1$	$\tan \delta = 1$	$\tan \delta < 1$	$\tan \delta \rightarrow 0$
$G' \rightarrow 0$		$G'' > G'$	$G' = G''$	$G' > G''$	$G'' \rightarrow 0$

The complex shear modulus G^* describes the relation between the time-dependent shear stress τ and shear strain γ , therefore the entire viscoelastic behavior of the sample:

$$G^* = \frac{\tau(t)}{\gamma(t)} \quad (7)$$

To interpret the obtained results, the storage modulus G' and the loss modulus G'' are derived (10)

from the shear strain and the shear stress. The storage modulus represents the elastic behavior of the sample. For elastic behavior, the energy is stored in the sample during shearing. Upon relaxing this energy will be released again. This process is reversible. On the other hand, G'' describes the viscous properties of the sample. Here the energy is lost during shearing and the energy either dissipates into the sample or surroundings or changes the structure of the sample, which is irreversible. The loss factor $\tan \delta$ relates the two moduli through their ratio thus indicating how dominant the viscous part of the viscoelastic behavior is in comparison with the elastic part in a given material. For interpretation of $\tan \delta$ consult table. G' , G'' and $\tan \delta$ are described with following equations, cosines and sine resulting from the phase shift δ , describing the viscoelastic behavior:

$$G' = \left(\frac{\tau_A}{\gamma_A} \right) * \cos \delta$$

$$G'' = \left(\frac{\tau_A}{\gamma_A} \right) * \sin \delta$$

$$\tan \delta = \frac{G''}{G'}$$

In oscillation experiments τ_A describes the shear stress amplitude and γ_A the deformation amplitude. (Mezger, 2016)

2.4.2.1 Amplitude - Sweep

Amplitude Sweeps are measured at constant frequency's (10 rad/s in industry labs) and temperatures with oscillating and over time increasing amplitudes. It is called a strain sweep if the deformation amplitude is the variable and a stress sweep if the shear stress is the variable.

An amplitude sweep is usually performed beforehand to determine the linear viscoelastic range (LVE-range). The LVE-range describes the range in which G' and G'' display a constant plateau value and run parallel to each other Figure 20. This results from the proportionality of the stress and strain parameter at small amplitudes, at amplitudes beyond the LVE-range no proportionality is given and a phase shift will be observed. The constant plateau of G' and G'' also implies that the measurement is non-destructive within this range, since there is no change in the phase shift. As G' usually tends to drop earlier than G'' , former is often used to determine the yield point γ_L , the x-axis intercept, at which the structure changes irreversible, before that reversible- viscoelastic behavior is to be assumed. Mezger (2016) suggested a deviation of 5 % from the plateau value for the determination of the yield point. Information of the sample can be derived from the relative position of G' to G'' . $G' > G''$ implies a solid or gel-like state and $G' < G''$ implies a liquid or sol-like state. In case of a sample where $G' > G''$ holds within the LVE-range, but $G' < G''$ is observed for higher frequencies, the point where $G' = G''$ is called the flow point γ_F . At this point the structure of the sample changes completely and it starts to creep or flow. The area between the yield point and flow point is called the yield zone or yield/flow transition range. The sample still shows solid characteristic but deforms already irreversible. A ratio of (γ_F/γ_L) can be calculated. This so-called flow transition index indicates the breakage behavior. The closer to 1, the more brittle is the sample.

Sometimes a maximum of G'' is observed, before the graphs start to fall, which is characteristic for highly concentrated dispersions with some form of network. The rise of the loss modulus indicates that, before

the final collapse, deformation energy is consumed to irreversibly deform some parts of the inner structure. The amplitude test can be used to observe the network stability of a system. (Mezger, 2016)

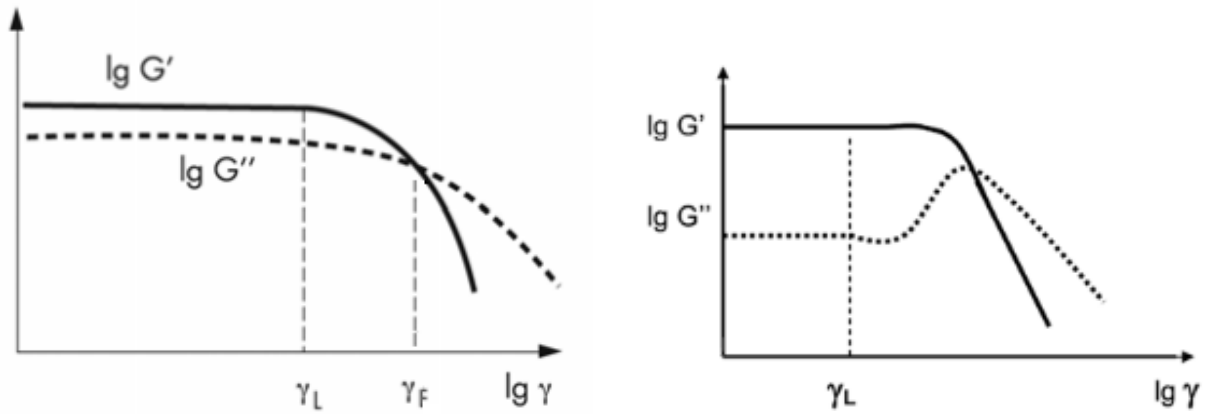


Figure 20: Amplitude sweep with γ_L as the threshold for the LVE-range. γ_F being the flow point with the sol/gel-transition, on the right side an amplitude sweep with G'' -maximum; modified after Metzger, 2016

2.4.2.2 Time-Dependent under Crystallization

A time-dependent measurement is done to monitor chemical or physiochemical reactions influencing the structure, in this case the crystallization of a fat. In absence of any reactions it is done to observe the effect of shear on the structure, as it is done under constant dynamic-mechanical conditions, meaning, with a constant parameters without permanent destruction of the sample's inner structure.

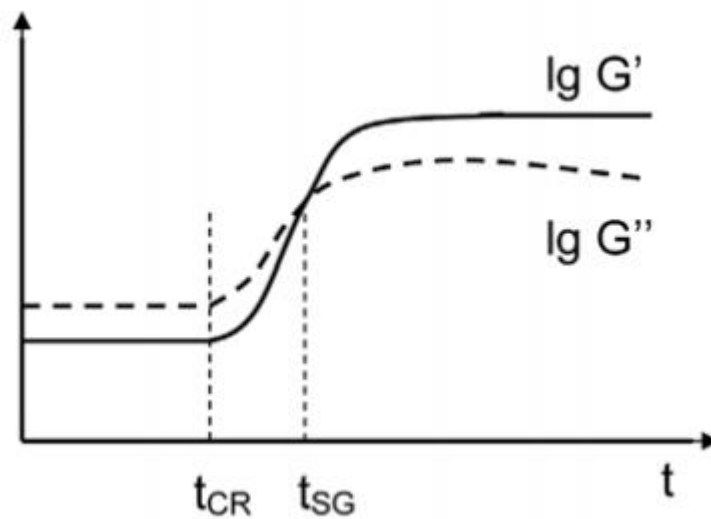


Figure 21: Time-dependent functions of G' and G'' of a curing process, with the time t_{cr} at the beginning of the phase transition and the time t_{sg} of the sol/gel transition at the intersection point $G' = G''$ (Mezger, 2016)

Curing of the sample can be observed as a rise of G' and G'' with the progression of time, for example due to crystallization. The starting point of the major crystallization process is referenced as t_{cr} in Figure 21, before that a plateau is shown, where no crystallization occurs. The point of intersection of G' with G'' is

the sol/gel transition t_{SG} . After some time, the curves flatten asymptotically, reaching their final constant value with $G' > G''$, for crystallization. Although further changes might occur as crystals might change to more stable polymorphs. Thus, there might be another change of the relative positions of G' and G'' . A sample might first display liquid tendencies with $G' < G''$, and if later the storage modulus and the loss modulus switch their position, the crossing point at which $G' = G''$ is denoted as sol/gel transition t_{SG} (Mezger, 2016).

2.4.2.3 Frequency Sweep

The frequency sweep is usually carried after determining the LVE-range and is measured at a constant amplitude inside the LVE-range and temperature. The oscillation frequency on the other hand is increased over time, while oscillating (dynamic oscillation).

A frequency sweep is usually performed to observe the time-dependent deformation behavior of a material. As the frequency is the inverse of time, high frequencies simulate fast movements on short timescales and low frequencies simulate slow movements on long timescales. It can also be used to observe possible superordinate or subordinate structures influencing a system, such as molecule interactions or networks. Depending on the Network the deformation is either large or small (Mezger, 2016). In case of cacao butter a three-dimensional crystal network at a microscopic level is formed and

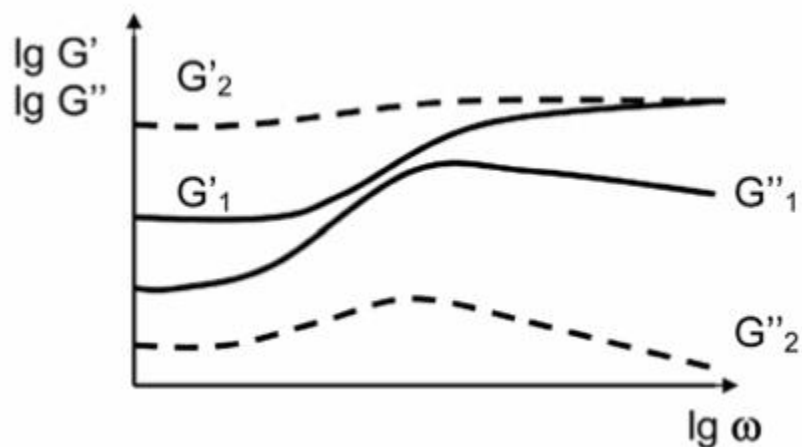


Figure 22: Frequency test of two networked polymers. 1 being only slightly connected, 2 a strongly connected polymer (Mezger, 2016).

could be observed with the frequency sweep. Because the frequency sweep is performed in the LVE-range, substructures below that of the microscopic level, such as TAG structure or individual crystal structure, are usually not affected (Narine & Marangoni, 1999).

2.4.3 Properties Influencing Rheology of Emulsions

One property influencing the rheology of emulsions is the packing of particles in the emulsion. Following simplified assumptions are made if there are no long-range colloidal interactions. The packing differs depending on the disperse-phase volume fraction ϕ of the dispersed droplets in the emulsion, as seen in Figure 23.

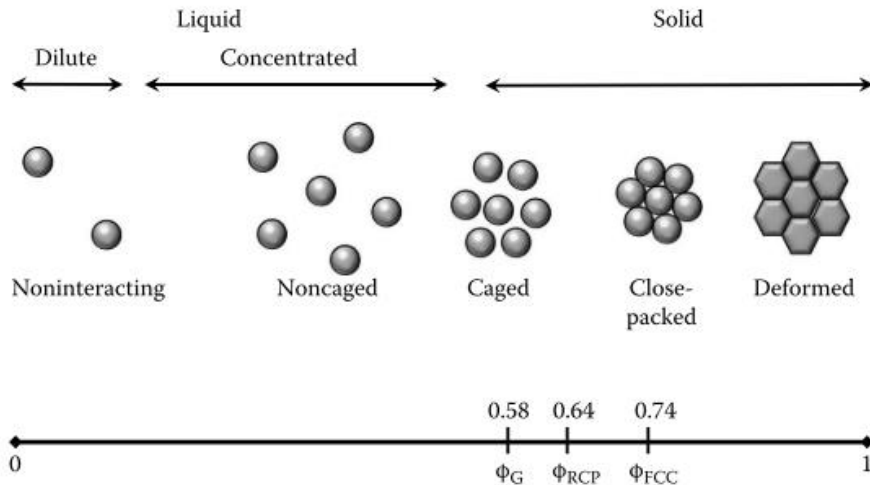


Figure 23: Display of disperse-phase volume fraction (ϕ) systems, ϕ_G = begin glassy systems; ϕ_{RCP} = random close packing, begin crystalline systems; ϕ_{FCC} = face centered cubic packing (McClements, 2010).

In diluted systems the droplets do not interact with each other. At $\phi < \phi_G$, the disperse phase volume being below the volume for glassy systems ϕ_G than the in the concentrated range, particles interact through hydrodynamic interactions, as well as particle collision and form a distinct crystalline (closely packed particles) and a fluid (loosely packed particles) phase, the closer the disperse-phase volume fraction approaches ϕ_G . Above ϕ_G , so called glassy systems are formed, where particles are restricted in their movement through their neighbors; they are “caged”, without being able to move past each other. Emulsions with this disperse-phase volume fraction can exhibit solid-like behavior at low shear stress and fluid-like behavior at high shear stress, after a sample specific critical yield stress is passed, which allows the particles to move past each other. ϕ_{RCP} marks with random close packing the beginning of crystalline systems. At $\phi > \phi_{RCP}$ the particles are packed so closely together that under shear they behave like an elastic solid. If the particles are soft, deformation can occur. Furthermore, there is a difference between monodisperse and polydisperse Systems, as monodisperse Systems are only able to achieve a maximum packing density of 74 % (closed packing), before deformation occurs. On the other hand it is possible for polydisperse Systems to achieve a much higher packing density through random packing, with smaller spheres filling the space between larger spheres, increasing the viscosity of the observed System. (McClements, 2010)

Another influence is any kind of colloidal interactions, for example electrostatic, steric, hydrophobic or van der Waals interactions. These, either repulsive or attractive interactions, influence the effects of the components of the emulsion at each other, changing the effective volume fraction, causing denser packing than actually possible with the actual volume fraction. Also if the volume-specific surface rises with a smaller droplet-average, so does the amount of interaction between the droplets, influencing the flow behavior. (McClements, 2010)

The viscosity of a fluid emulsion is directly linked to the viscosity of its continuous phase. The viscosity of the dispersed phase usually does not influence it, as the droplets are covered in a viscoelastic emulsifier layer and seen as rigid spheres. Only large droplets might influence the viscosity of the system, as they are easier deformed under stress, allowing the droplets to pass each other, lowering the viscosity.(Derkach, 2009)

Physiochemical change also influences the emulsion, for example as fat solidifies under different temperatures, a crystal network appears, jamming and increasing the viscosity. (McClements, 2010; Mezger, 2016). The TAGs of cocoa butter form a three dimensional crystal network, which macroscopic rheological properties are influenced by the structure of the individual TAGs, the individual structures of the formed polymorphous crystals and their linkage to other crystals (Narine & Marangoni, 1999). Single TAGs form through stacking lamellae and form with their chain length structure in the sub cell structure (domain) single crystallites. These single crystals agglomerate and are part of a bigger solid primary particle, which is dispersed in liquid oil. The primary particles form a random network, which on a fractal scale is divided into blobs. The size of this blob depends on the degree of crystallinity (the solid fat content), decreasing with increasing degree. Multiple blob-sized network pieces are linked together into a crystal network, forming the bulk seen on a macroscopic scale. The strength of the network determines the shear at which the network or even the blobs at higher shear will break apart. At this point the system will become liquid and will begin to flow. (Vilgis, 2015)

This structural hierarchy of fats is shown in Figure 24.

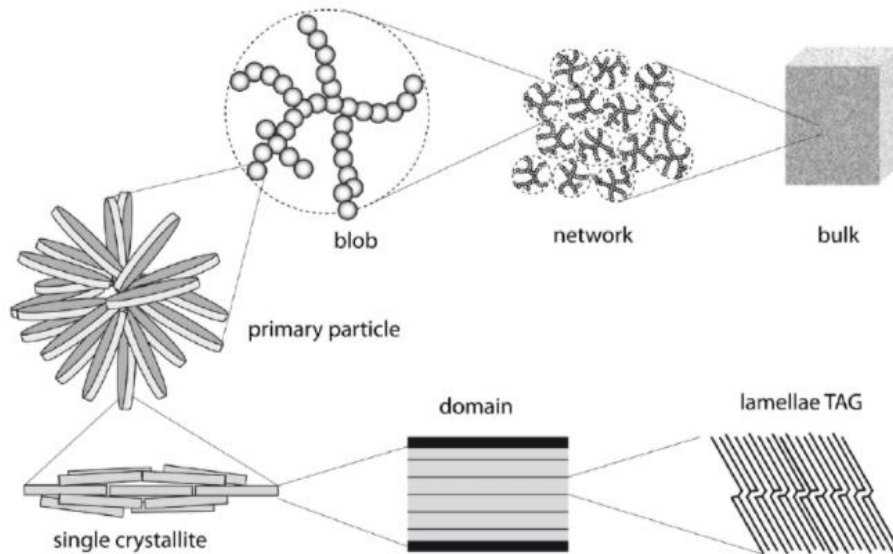


Figure 24: Solid fat at various length scales (Vilgis, 2015)

3 Material and Methods

3.1 Material

The materials as well as the selected are presented in the following chapter.

Pure water from a Milli-Q®-plant was used for all experiments.

Cocoa Butter

The cocoa butter (CAS-number 8002-31-1) used was purchased in the form of pure, double filtrated, light yellow pellets from Carl Roth GmbH + Co. KG. The same charge was used for all experiments. According to the analysis report the charge has a melting point of 32 °C and a density of 0.96 g/cm³.

Soy Protein Isolate

The powdered soy protein isolate VEGACON® 90 was provided by EUROSOY GmbH. It is made from NON-GMO soybeans. The same charge was used for all experiments and contains, according to the assessment report of the company 92.5 wt% protein, 6.4 wt% water and 4.7 wt% ash. The rest are minor components.

Soy Milk

The used soy milk 'Soja Drink ungesüßt' was purchased from a local organic food supermarket, Alnatura, and contains 9 wt% soybean and 91 wt% water according to the package.

Sodium Dodecyl Sulfate (SDS)

The surface-active sodium dodecyl sulfate (SDS) with the CAS-number 151-21-3 from Carl Roth GmbH + Co. KG was used.

Sodium Chloride (NaCl)

Sodium chloride (NaCl) with the CAS-number 7647-14-5 was purchased from VWR.

3.2 Methods

In the following chapter the selected methods are presented. All steps for sample preparation were performed at room temperature except if noted differently.

3.2.1 Emulsion Preparation

To prepare the emulsions, cocoa butter (55, 60, 70, 75 wt%) was melted for one hour at 90 °C to remove all crystal memory, meaning removing as many seed crystals as possible. The soy protein isolate (SP) - water dispersion (3, 4, 5 wt%) was stirred for one hour to form a homogenous dispersion. In the case of soy milk emulsions, no special prior treatment was given to the soy milk. After one hour the SP dispersion or soy milk was added to the molten cocoa butter. The two-phase system was then emulsified by an ULTRA-TURRAX® T 18 basic with the S18N-19G dispersing tool from IKA, following the rotor/stator principle. All 25g emulsions were prepared at a speed of 7.200 rpm (idle speed) and a homogenization period of 3 minutes. For transport the sample was kept in an insulated sample container to keep the internal temperature of the emulsion above the temperature at which measurements were performed.

3.2.2 Light Microscopy

Microscope pictures of the prepared emulsions were captured with the help of the light microscope Axio Scope.A1 from the Zeiss. Polarized light was used to observe the crystal growth over a period of three hours at 22 °C accordingly to the time-dependent rheometry measurement. Under polarized light anisotropic solids refract light differently than an isotropic liquid phase (Zeiss, 2009). The solids appear

white, liquids black, the contrast depending on the chosen angle., which was either 0° or 45°. Temperature-ramps from 22 °C to 40 °C to 22°C with 0.5 °C/min steps were performed to observe the stability of the emulsion under heat treatment. Objectives with 10, 40 and 100x magnification were used. ImageJ was used to insert the scale.

3.2.3 Laser Diffraction Particle Size Analyzer

The droplet size distributions of emulsions were determined by a laser diffraction particle size analyzer (LS 13320 of the company Beckman Coulter) in a stirred fraction cell. A 5-mW-laserdiode with a wavelength of 750 nm (or 780 nm) is used as primary light. The measuring range of the instrument is between 0.040 and 2000 µm due to data analysis using a combination of laser diffraction and Mie scattering theory, with every particle size fraction scattering the light in a characteristic angle. A Fourier lens bundles the rays and enables the scattering pattern to be recorded by detectors. The detector is divided in channels, each channel recording a specific particle size fraction. As the particles are moving in the cell, different scattering patterns are recorded over time. From the measuring time an analysis of the intensity measured in each channel reveals the actual particle size distribution of the sample. It is an indirect method to determine the particle size of a sample and uses mathematical models for the analysis. Here the used model was based on the Fraunhofer-theory. This model does not require any additional data such as refractive index or absorption coefficient for the calculation performed by the included computer program.

It is also possible to measure particles in the nanometer range (starting at 10nm) with the help of PIDS (Polarization Intensity Differential Scattering) technology. The PIDS-system uses a secondary tungsten-halogen-lamp in combination with polarization filters. The acquired wavelengths are 450nm, 600nm and 900 nm.

The whole measurement is a combination of PIDS and laser diffraction. The analysis was done with the included computer program.

To ensure the reproducibility of the particle distribution, the emulsion must be diluted. The dilution was carried out in a ratio of 1:99 (0.1g sample, 9.9 g 1% SDS-Solution with 60 mmol/L NaCl). This solution composition was chosen through comparison of microscope pictures and particle size measurements. The dilution was carried out immediately after emulsion preparation and measured as soon as possible, to additionally minimize the possibility of aggregation or creaming. The instrument was calibrated before each measurement, including rinsing, debubbling, background measurement and aligning of the measurement cell. The graphical evaluation was performed in the OriginPro 2019b graphics software.

3.2.4 Rheometry

For the rheological measurements the Discovery Hybrid Rheometer (DHR3) from TA Instruments was used. All settings on the rheometer were adjusted using the TRIOS software provided by the manufacturer, version 5.1.1. During the measurements, a solvent trap was used to prevent water evaporation. The temperature was controlled with the help of a Peltier Temperature Control System and kept at 22°C. The evaluation of the data was carried out using OriginPro 2019b. A triple determination of the measurements was performed of emulsions prepared with a 60 wt% oil-volume fraction.

For the measurements a parallel plate-plate geometry with a diameter of 20 mm and a gap size of 1 mm was used.

The following settings, listed in the Table 4: Settings used for rheological measurements. below, were used for the rheological measurements. Those were measured at least 3 times per sample. Furthermore, for comparison, single measurements were taken from 60CB_3SP at 4°C (2h, 3h, 24h) and 25° (2h) though,

for reasons of time, further repetitions could not be carried out. However, it would be interesting to study them further in the future.

Table 4: Settings used for rheological measurements.

Methods	Temperature [°C]	Shear strain γ [%]	Angular frequency ω [rad/s]
Time-Dependence (3h)	22	0.01	10
Frequency-Sweep	22	0.01	0.1 -100
Amplitude-Sweep	22	0.001-1000	10
		Shear rate $\dot{\gamma}$ [rad/s]	
Controlled Shear Rate (CSR)	22	0.1 - 1000	

Time-dependence observation was immediately followed, without removing the sample, by the frequency sweep and amplitude sweep. Each emulsion sample was made with a freshly prepared soy protein solution, if the measurement of the same concentration was done another day. A CSR was performed with freshly prepared SP60CB-emulsions and SP-dispersions. Upon applying the sample on the rheometer, the emulsion rested there at a static position for about 10 minutes at 22°C before starting the CSR.

3.2.5 Pressure-Test

A pressure test was performed with the help of a Zwick Roell Z004. For sample preparation freshly prepared emulsion was poured into molds, resulting the next day in cylinders with a diameter of 15.7 mm and a height of 22.3 mm. A “Two-Bite”-test was performed. The samples were compressed at a speed of 1 mm/s with a 40 % strain of the pre-compression height. Two cycles were performed, with no resting time in between the samples.

3.2.6 Data Analysis

The average was calculated for any series of data, as well as the standard deviation of the average, which were included in the graphs as error bars.

Since loss and storage modulus are usually plotted logarithmically for analysis, the error estimation Δy via standard deviation $\sigma(y)$ has to be adjusted accordingly, so that a reasonable approximation is displayed symmetrically for the logarithmic values. This was achieved by plotting the logarithm of the G' and G'' on a linear scale and calculating the error bars as follows:

$$\Delta y = \frac{\sigma(y)}{y * \ln 10} \quad (11)$$

The size distribution was measured as relative volume of particles. The data that are reported in this thesis are the diameter of which 90 % of the particles are smaller (D_{90}), the median (D_{50}) and the diameter of which 10 % are smaller (D_{10}). With those values the span of the distribution (s) is calculated. Also the volumetric-length mean ($D_{4,3}$) and the mode (D_{mode}), the most common diameter are given.

To determine the reported values t_{cr} and γ_L a linear fit was laid in a suitable interval (choosing the middle area) through the linear area values and the x – value of the data point first deviating by 5 % from the linear fit were determined as the reported values. The loss factor $\tan \delta$ was calculated with equation 10.

4 Results and Discussion

In the following, the results from observing the soy protein stabilized cocoa butter emulsion will be discussed. The emulsion is observed in its liquid and solid state using various methods. First the general aspects of the components and the macroscopic and microscopic structure of the emulsion will be discussed. The effect of different oil proportions, dilution, emulsifier concentration, time and measurement temperature were observed.

4.1 General Description

A general description of the used materials and emulsion and the effects of different emulsion preparations on the macroscopic stability will be given in this chapter. The melted cocoa butter is



Figure 26: Soy protein dispersions with different soy protein content. Upper: 1 wt% SP, Lower: 10 wt% SP

transparent and of a bright yellow color (see Figure 27 a). The pure soy protein solutions are of a light brown color with a gel-like texture, especially with rising soy protein content. In Figure 26 the difference in texture between a 1 wt% soy protein dispersion and a 10 wt% one is shown. A homogenization period of 3 min with a speed of 7200 rounds/s with a head-diameter of 19 mm were chosen, as less resulted in separation of the emulsion in less than 30 min. This can be seen in Figure 25. No uniform white-light yellow color was achieved, and the phases are seen to be separating (different colors) at the top and bottom of the samples. Even if the sample prepared with the 10 wt% had an emulsifier-rich environment, which could have been the explanation for the phase separation of the sample prepared with the 1 wt%, the mechanical energy infused into the system was not enough to form a kinetically stable emulsion, as only a few droplets were formed.

With the above mentioned settings of the homogenizer a non-phase separating emulsion was accomplished, provided that it was kept at room temperature or below. If prepared at 40 °C and kept at this temperature, breakage of the emulsion could be observed. This occurred in the form of oil droplets appearing on the surface, while a skin was formed. The main body of the emulsion sometimes remained unchanged and sometimes separated as well. No reproducibility was achieved. A problem was probably that the sample in the oil bath was subjected to temperature fluctuations, destabilizing the formed emulsion. If the emulsion was allowed to cool down during the homogenization process, as it was the case if prepared outside of an oil bath without temperature control and as the finished sample were kept at room temperature, a non-separating emulsion was achieved. With the latter method the finished emulsions had an internal temperature of 34 ± 2 °C, were opaque and of a light yellowish color and were able to flow. Under the microscope the individual droplets can be distinguished and a polydisperse distribution of the droplets can be seen, with smaller droplets filling the



Figure 25: Phase separation after 30 min because of lacking mechanical energy. Left: CB emulsion prepared with 10 wt% SP; Right: CB emulsion prepared with 1 wt% SP.

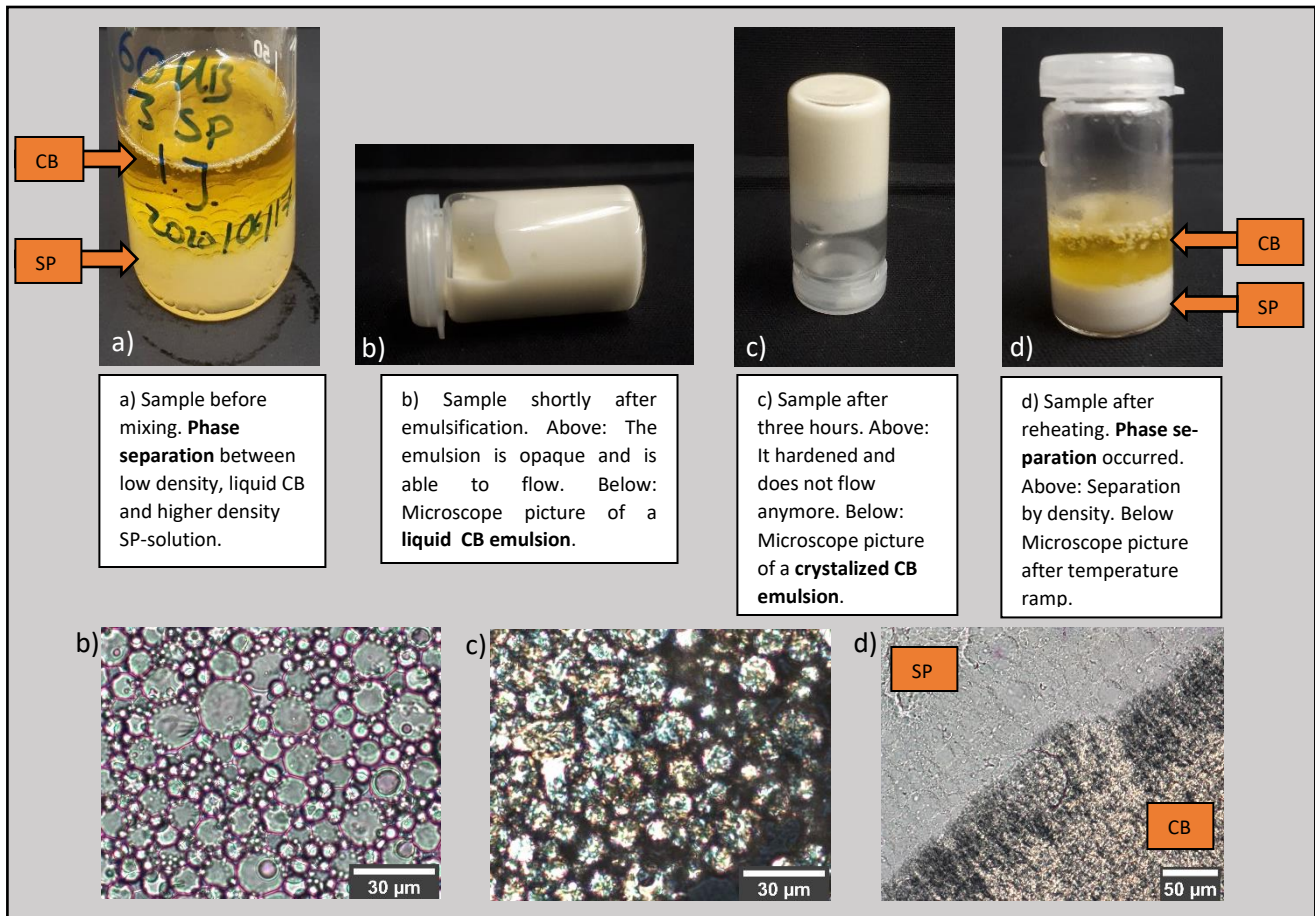


Figure 27: Pictures and microscopic images of emulsion before (a) and after (b) emulsification, as well as after crystallization (c) and reheating (d). SP = Soy protein, CB = cocoa butter

space between larger droplets, see Figure 27 b. This incorporation of the oil phase into the watery phase is a clear difference to the phase separation observed before emulsification in Figure 27 a.

During 3-4 hours the emulsions kept at room temperature had hardened and did not flow anymore along the pull of gravity, see Figure 27 c. The hardening could also be seen because of a slight color change to a lighter yellow, similar to the color of the used cocoa butter pellets. Bulk hardened more slowly than thin layers. The hardening of the emulsion resulted from the crystallization of the oil phase. Additionally, as seen from microscope images, the assumption that proteins form oil-in-water emulsions is confirmed, as crystallized droplets could be observed surrounded by liquid, with the help of polarized light. In polarized light under certain angles anisotropic solids appear white, while isotropic liquids appear black, as it is seen in Figure 27 c. Little to no contraction was observed. Contraction behavior usually depends on the formed polymorph, which could be adjusted through tempering of the cocoa butter (Garti & Aserin, 2012; Narine & Marangoni, 1999). As emulsions destabilizing upon heating, a conventional tempering process used for chocolate would not be feasible and would be needed to be done before emulsification. Through to the here used emulsification process, the formation of polymorphs probably depends more on the cooling rate and additives, in this case the soy protein. Under pressure the hardened samples showed brittle behavior. As seen in Figure 27 c, when a hardened sample was reheated, phase separation could be observed not only macroscopic but also through microscopic pictures, where the cocoa butter forms an extended area, expelling the water phase. On a macroscopic level this is explained through the different

densities of the oil- and water phase, although the question still remains why the crystallized droplets do not simply return to their liquid state and remain stable. A possible explanation for such behavior could be described through the protein adsorption rate and occurrence of partial coalescence and will be discussed in detail in a later chapter (4.4).

4.2 Droplet Description

4.2.1 Effect of Oil Content

Emulsion with an oil content ϕ of 55, 60, 70 and 75 wt% were achieved. On a macroscopic level no specific difference between the emulsions could be observed, except the samples seemed to be more viscous with rising oil-content. Microscope pictures of the emulsions can be seen in Figure 28. The emulsion with $\phi = 55$ wt% and $\phi = 60$ wt% showed spherical droplets, while emulsions with an oil-fraction of $\phi = 70$ wt% showed slightly ellipsoidal droplets, whereas $\phi = 75$ wt% emulsions showed strongly deformed ellipsoidal droplets. The deformation probably stems from the fact that the former two are below and the latter two are above the disperse-volume fraction $\phi_{RCP} = 64$ wt% at which deformation might occur, see chapter 2.4.3. 55 wt% is right below the fraction for begin of the glassy systems $\phi_G = 58$ wt% in the partially crystalline systems fraction. On the microscope picture the two large droplets seen are the fluid phase, filled with only loosely packed droplets, while the surrounding area is filled with densely packed droplets, forming the crystalline phase. The microscope images explain the observed rise of viscosity of the samples, as it is harder for closely packed and deformed particles to move past each other than for less densely packed and not deformed particles. With this the models described in literature, see theory chapter 2.4.3,

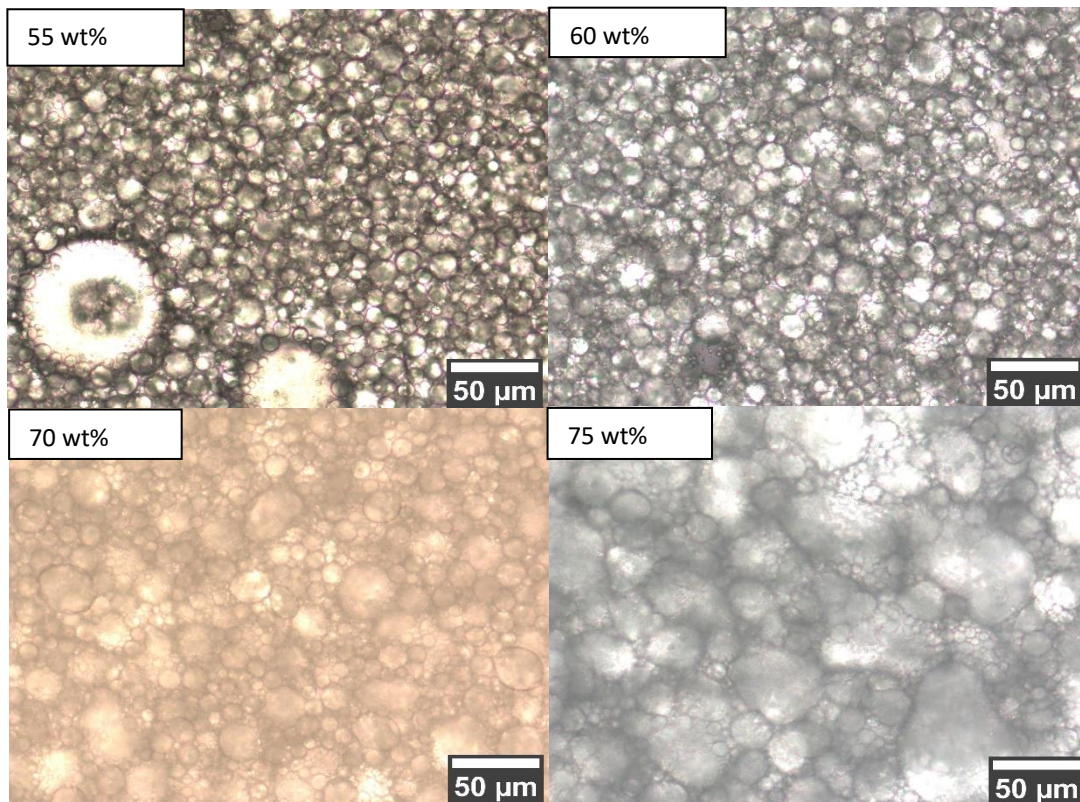


Figure 28: Microscope pictures of CB emulsions with $\Phi = 55, 60, 70, 75$ wt% CB content prepared with a 4 wt% SP-dispersion.

could be verified. The rise in the overall size probably derives from the fact that for all four emulsion types

4 wt% SP-dispersions were used. With this the concentration of the emulsifier in the continuous phase stayed the same, but with rising oil content the available emulsifiers in the whole sample decreased with the decreasing volume of the continuous phase. As such, the emulsifier was not able to cover as much surface as before, resulting in larger droplets with less surface. The effect of emulsifier concentration was further investigated through the help of particle size measurements.

On the basis of these observations $\phi = 60$ wt% was chosen as the oil-fraction for all further investigation. Because of the possible droplet deformation 70 and 75 wt% were disregarded, as the Fraunhofer theory used for the data-analysis of the particle size measurements assumes a spherical shape of the measured droplets. 55 wt% was not chosen as it contained two distinct phases making it unsuitable for rheological measurements.

4.2.2 Dilution Stability

Creaming of the homogenized emulsion occurred if no emulsifier was added or if the emulsion was diluted with water, see Figure 30. Creaming, caused by the different densities of the contained phases, is often preceded by flocculation or coalescence, which are influenced through the electrostatic and steric properties of the used surfactant, as explained in chapter 2.3. These phenomena could also be observed through measurements with the particle analyzer, Figure 29.



Figure 30: Creaming of with water diluted emulsion.

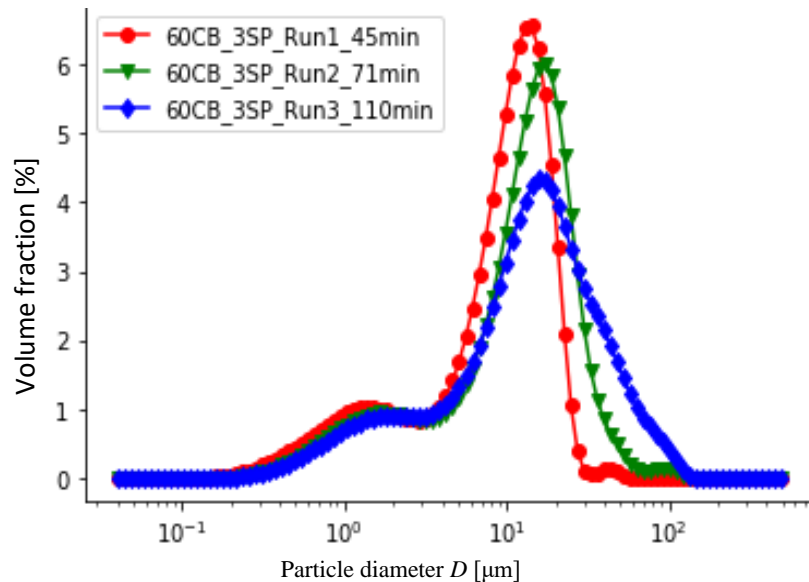


Figure 29: Changes of particle size distribution of water diluted CB-SP-emulsions over time.

A sample diluted with water was measured three times over an interval of two hours. As seen in Figure 29 the width of the particle distribution enlarges over time suggesting some kind of agglomerations are happening. Additionally if observed under the microscope it can be seen (Figure 32, left), that the droplets are not spherical anymore. This makes water as dilution medium unsuitable, as precise measurements for particle size distribution would be difficult to achieve.

To avoid aggregation of the oil droplets in the water phase sodium dodecyl sulfate (SDS) was added as an additional surfactant. As seen in Figure 31, SDS has a hydrophilic head and a hydrophobic tail. The amount

of the hydrophilic parts can be controlled by adding sodium chloride.

Figure 32 (middle, right) shows the difference between water, 1 wt% SDS-Solution + 80 mmol NaCl and

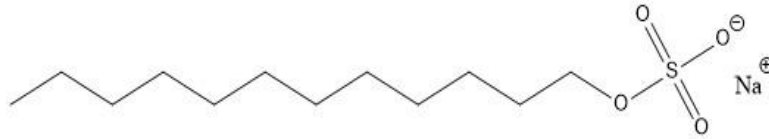


Figure 31: molecular structure of sodium dodecyl sulfate (SDS).

1 wt% SDS-Solution + 60 mmol NaCl. Latter showed the least amount of agglomeration, improving the accuracy of the particle distribution in order to achieve precise measurements. Therefore to prepare a sample for the particle analyzer, the sample was diluted in a ratio of 1:99 with a 1 wt% SDS-solution + 60mmol NaCl.

To improve the accuracy of the distribution further, the sample was measured as soon as possible after

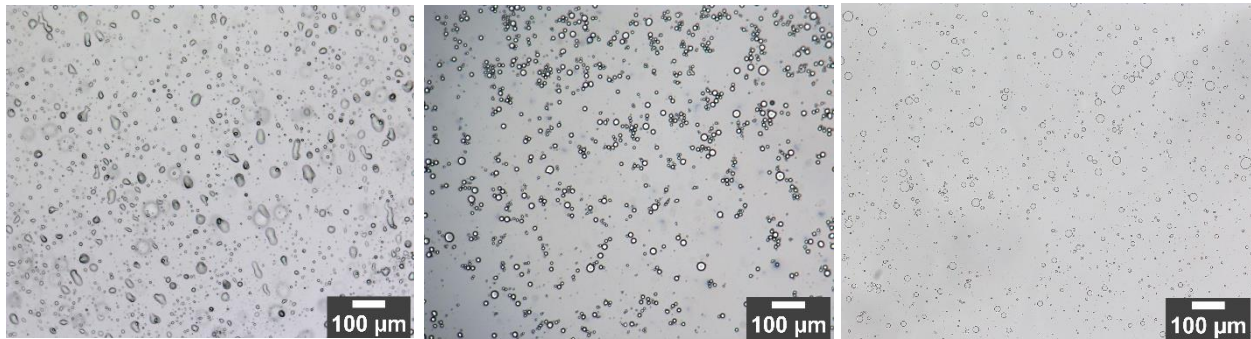


Figure 32: Comparison of different dilution (1:99) compositions; Left: Water; Middle: 1 wt% SDS-Solution + 80 mmol NaCl; Right: 1 wt% SDS-Solution + 60 mmol NaCl.

preparation, as with increase in waiting time, the sign of flocculation was observed for some measurements. For instance, in Figure 33, the distribution width of a measured 60CB-3SP sample is unchanged and peak placement is detected at the same position for the sample. After a period of about one hour passed, however, the peak height increased, indicating an increase in the most common diameter size., through either flocculation or coalescence of the smaller droplets. One extra peak was detected at larger diameters after 22 min (green graph, inverted filled triangle symbol), which was not detected for the following measurements, which hints for either flocculation or air bubbles. As such those might not be part of the actual size distribution, especially as non-such large droplets could be found through the microscope. Although the microscope is only a small window to the whole emulsion.

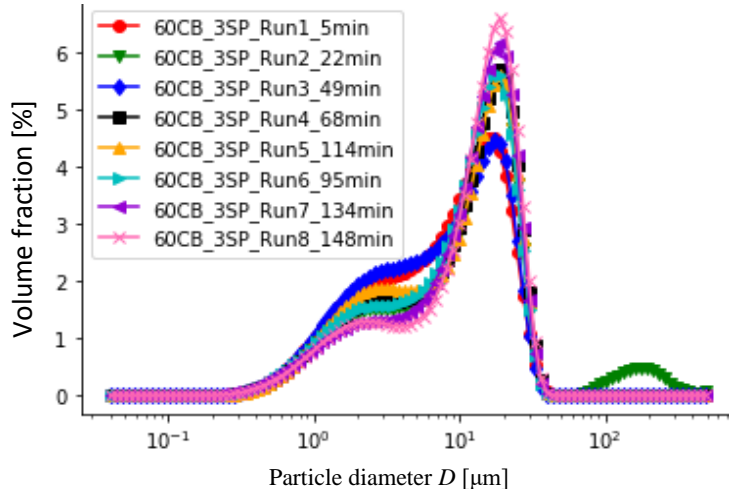


Figure 33: Changes of particle size distribution of 1 wt% SDS-solution + 60mmol NaCl diluted 60CB-3SP-emulsions over time.

4.2.3 Particle Size Distribution

For all following experiments, an oil-fraction of 60 wt% and SP-dispersions with 3, 4 and 5 wt% SP were used. Microscope pictures (Figure 34) show polydisperse systems and a decrease in droplet size with rising SP-content.

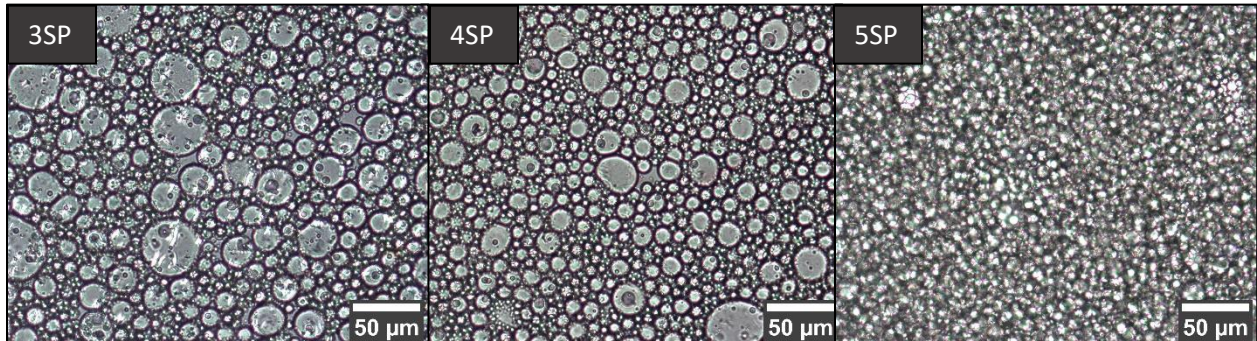


Figure 34: Microscope pictures of CB-SP-emulsions prepared with left: 3 wt%, middle: 4 wt%, right: 5 wt% - SP dispersions at a magnification of 40x.

This trend could also be observed through measurement of the particle size distribution (Figure 35) with the help of a particle analyzer, which measures a volume weighted diameter contrary to microscope pictures, which show a number-weighted diameter. The mean diameters would be the same if a monodisperse droplet distribution was measured, but this is not the case for a polydisperse system. The span s , calculated from the D-values, describes the polydispersity of a system.

$$s = \frac{D_{90} - D_{10}}{D_{50}} \quad (12)$$

The number subscript of the D-values describes what percentage of the droplets is below the given diameter of the D-value. In an ideally monodisperse System D_{90} and D_{10} would be the same as the median D_{50} yielding $s = 0$. The different CB-SP emulsions on the other hand had a similar span of $1,99 \pm 0,4$, far off a monodisperse emulsion. The polydispersity of the system explains the discrepancies between the

microscope pictures, which show a large difference between the droplet sizes of the emulsion prepared with 4 wt% and 5 wt% SP and the fairly similar mean diameters of 8.25 μm (4SP) and 7.59 μm (5SP), see Table 5. It also might be because of the different emulsion preparation, as the particle analyzer measures a diluted system instead of a concentrated one.

Table 5: Description of the droplet size distribution with different values.

	Mean $D_{4,3}$ [μm]	Mode D_{mode} [μm]	D_{50} [μm]	D_{10} [μm]	D_{90} [μm]	Span s [1]
3SPCB	15.03	16.44	10.05	1.39	21.63	2.01
4SPCB	8.25	11.01	6.65	1.15	14.60	2.02
5SPCB	7.59	9.445	5.90	1.08	12.61	1.95

The measured particle size distribution shows a slight bimodal distribution with one distinct peak (mode) and a shoulder at lower diameters see Figure 35.

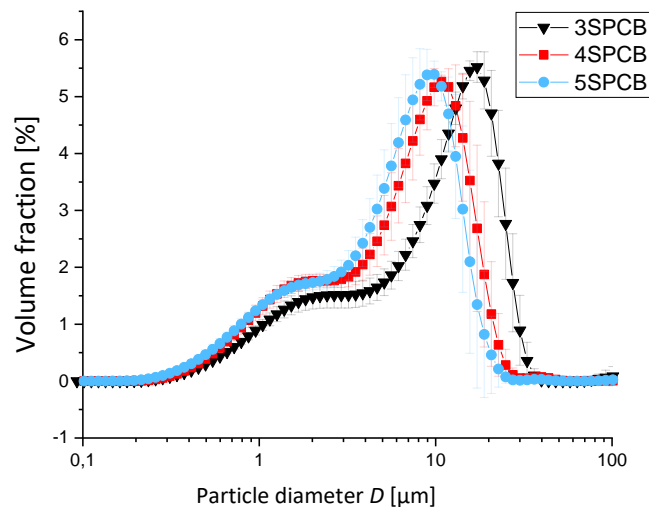


Figure 35: Droplet size distribution of CB (60 wt%)-emulsions with different SP-concentrations.

This shows, in combination with the microscope pictures, that larger droplets of a similar size are packed together, while smaller droplets fill the space in between the larger droplets, allowing a more efficient and denser packing of the space. As such, more disperse phase volume can be incorporated into the water phase. It is interesting to see that mode seem to shift more to smaller diameters with increasing SP-content than the shoulder does. A possibility is that the smaller droplets are formed in the beginning while there is still an emulsifier rich regime prevalent, with the homogenizer being the limiting factor. With increasing number of smaller droplets less emulsifier is available resulting in larger droplets. This would also explain the shift of the mode to smaller diameter sizes with increasing SP-content, as there is more emulsifier available to stabilize the increase of surface, assimilating with the homogenizer limited droplet diameters.

This is further supported by comparing the modes and mean diameters of the different SP-concentrations (Figure 36) shows for those three emulsions a non-linear decrease of droplet size, as suggested in Figure 11 (theory part 2.2.2). To ascertain if further concentration increase would lead to an asymptotic flattening of the curve, with the diameter size limited by the homogenizer, further experiments with

higher concentrations would be needed to be conducted. The general decrease of the average droplet size with increasing emulsifier content, shows that because more emulsifier is available a larger surface of the same oil-volume can be covered, resulting in stabilizing smaller droplets. The decrease of the droplet diameter for SP-stabilized emulsions with rising SP-content was also observed for SP-concentrations ranging from 0.5 wt% to 4 wt% by Tang & Liu, (2013).

Samples with Soy milk (SM) were prepared as well, but could not be analyzed through the particle

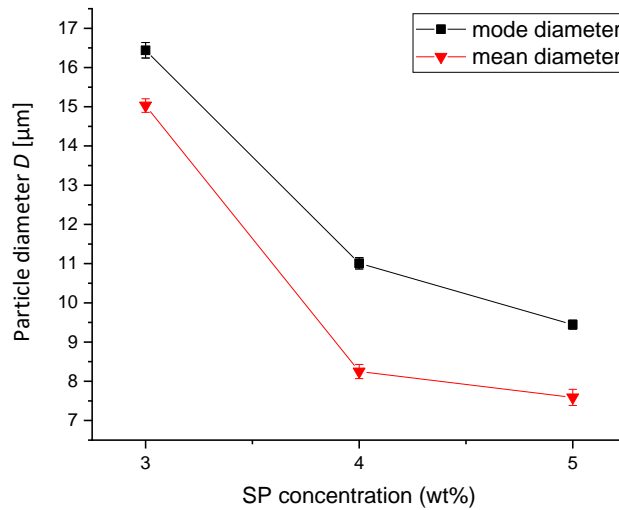


Figure 36: Mean and mode diameter of droplets weighted by volume with respect to SP-concentration.

analyzer, as the soy milk used, when performing the experiments, was not able to completely emulsify the CB, as seen in Figure 37 (middle). Some droplets are visible, but they are embedded in larger areas of CB. Dilution resulted in deformed droplets, changing the sample making it not usable for particle analysis, Figure 37 (right). Earlier obtained SM used in pre-experiments on the other hand was able to emulsify the CB (Figure 37 (left)), suggesting a change in emulsifier concentration in the SM. As mentioned in the theory chapter 2.2.1.1, concentration ranging from 1 – 4 % SP, were found in different SMs. Theories about emulsions cannot be directly applied to the samples prepared with the SM where a lot of CB is still in bulk.



Figure 37: Comparison between emulsion prepared with SM, purchased at different times. Left: Emulsion prepared with SM purchased for pre-experiments, middle: Emulsion prepared with SM purchased for experiments, magnification 40x left: Diluted emulsion for experiments, magnification 10x.

4.3 Flow Behavior of the Liquid Cocoa Butter Emulsion

The viscosity of the freshly prepared emulsions was measured with respect to shear rate and compared to the viscosity of the continuous phase, the SP-dispersions.

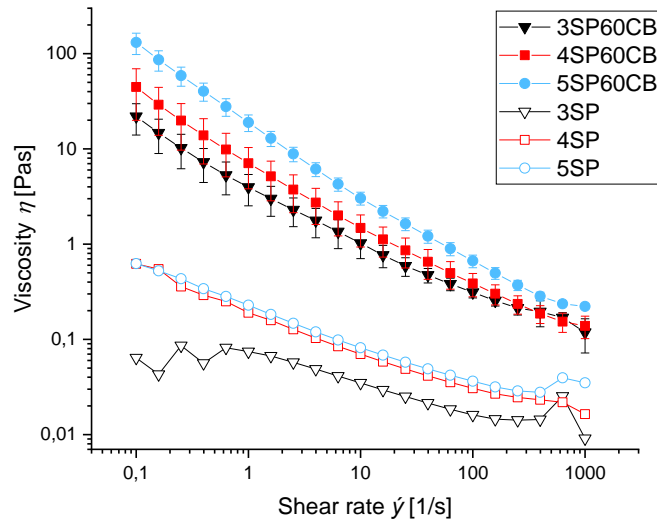


Figure 39: Viscosity curve of CB-SP-emulsions (full symbols) and SP-dispersions (empty symbols).

In Figure 39 the viscosity of the samples in dependence of the shear rate is shown. The viscosity of the continuous phase (3SP, 4SP, 5SP) is lower than that of the emulsions. In diluted systems the viscosity of an emulsion is determined through the viscosity of the continuous phase, but with a rising disperse-phase fraction the emulsion is influenced by the packing possibilities of the disperse phase, hence the higher viscosity of the emulsions. As already discussed in the section about the oil-content, the investigated emulsion with an oil-content of 60 wt% is classified as glassy system, see chapter 2.4.3 and 4.2.1. This is

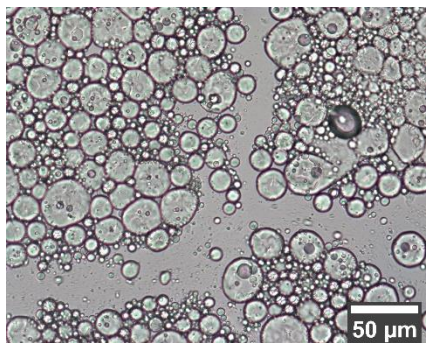


Figure 38: Observed flocculation in CB-SP-emulsions. Appearance of "water streets".

also supported by the shear thinning behavior which is concluded by the decreasing progression of the viscosity curve. At low shear-rate, the droplets are still "caged" by their neighbors. This is further increased through attractive interaction of the emulsifier layer causing flocculation and an even denser packing, see Figure 38.

With rising shear-rate the droplets are able to slide past each other, probably being deformed and hence the viscosity decreases. Another observation according to the result is as the SP-concentration decreases, the viscosity of emulsion decreases. Emulsions prepared with 3 wt% SP contain larger droplets than emulsions with a higher SP-content, as seen in 4.2.3. Larger droplets are deformed easier than smaller ones, packed less densely and the total surface decreases. With those possible interactions between the droplets, decreasing viscosity, from 5SP60CB emulsions with the highest values to 3SP60CB emulsions with the lowest values for the emulsions, can be explained. SP-dispersions also show a shear-thinning behavior, but the viscosity is not as high, as the SP is smaller than

the emulsion droplets, causing less friction. With rising SP-content more interactions, such as van-der-Waals forces, hydrogen bonding and electrostatic interactions, as well as hydrophobic effects of the amino acids, are possible between the sidechains of the amino acids in the proteins. Through those interactions macroscopic gel like structures (Figure 26) are formed, resulting in an increase of the viscosity. In the emulsion only the hydrophobic side groups of the amino acids will dissolve into the oil, changing the interactions.

4.4 Crystallization of the Emulsions

To observe the macroscopic observed curing process in more detail, time-dependent measurements of the freshly prepared emulsions were undertaken. These are performed with constant temperature, amplitude and frequency to observe changes of the moduli. As the liquid CB crystallizes, as observed under the microscope, an increase of the moduli was expected, which is confirmed according to Figure 40, where the rise of the storage modulus over time is shown. Crystallization in O/W-emulsions is usually heterogeneous (Hindle et al., 2000). Secondary heterogeneous nucleation can be further divided into a primary and secondary crystallization process for cocoa butter emulsions. The primary crystallization process is dependent on cocoa butter seed crystals remaining in the liquid cocoa butter after heating, being unaffected by the surfactants, with the seed crystals inducing crystallization at temperatures close to the bulk crystallization, with Hindle et al. (2000) determining a temperature of 14 °C for their cocoa butter emulsion. To avoid this process as much as possible, cocoa butter should be heated to above 80 °C to remove as much crystal memory as possible, because at 80 °C seed crystals exceeding the size of 0.28 µm still exists, although the average size was inferred to be less than 0.09 µm (Hindle et al., 2000). This was the reason why 90 °C was chosen as a melting temperature, although some high melting crystals might remain even at those temperatures. With few seed crystals remaining only a minority of the emulsion droplets will crystallize, as collisions between droplets without crystallized material are unlikely to crystallize. But the droplets containing crystallized materials can catalyze a secondary crystallization process, which is a collision mediated process, with fat crystals penetrating into liquid droplets, initiating crystallization and promoting partial coalescence.(Hindle et al., 2000)

These findings were supported by crystallization observed in this study. The crystallization was detected through a time lapse under the microscope and the times corresponded with the rheological measurement. The result of both methods is combined in Figure 40. The mainly liquid state of the emulsion, containing a small amount of seed crystals at the beginning of the measurement (t_{begin}), was continuously observed during the time frame corresponding to the low gradient linear range of the rheological measurements. The second microscope picture shown in Figure 40 was taken at $t_p \approx 3000$ s. The first two pictures shown in Figure 40 are taken with a polarization filter angle of 0° as it was easier to observe the droplets. Starting at approximately 4500 s the angle was switched to 45°, showing some crystal seeds, seen as bright spots, due to their anisotropic nature. Still liquid material is seen in dark colors. No major change was observed until t_{cr} , supporting the findings of surfactants influence on crystallization processes of Hindle et al. (2000). They observed that surfactants do not influence the primary crystallization process of CB, which is mainly influenced through seed crystals. Those promote crystallization at temperatures around 14 °C, which is below the measurement temperature and as such will not greatly influence the system. Complementary to heterogeneous secondary nucleation, which promotes crystal growth in the vicinity of chemical similar substance such as seed crystals, the amount of crystals, seen in the microscope pictures $t \approx 4500$ s seems to have increased at t_{cr} in the vicinity of before observed seed crystals. At t_{cr} a rapid crystallization process started, visible by the sudden rise of the

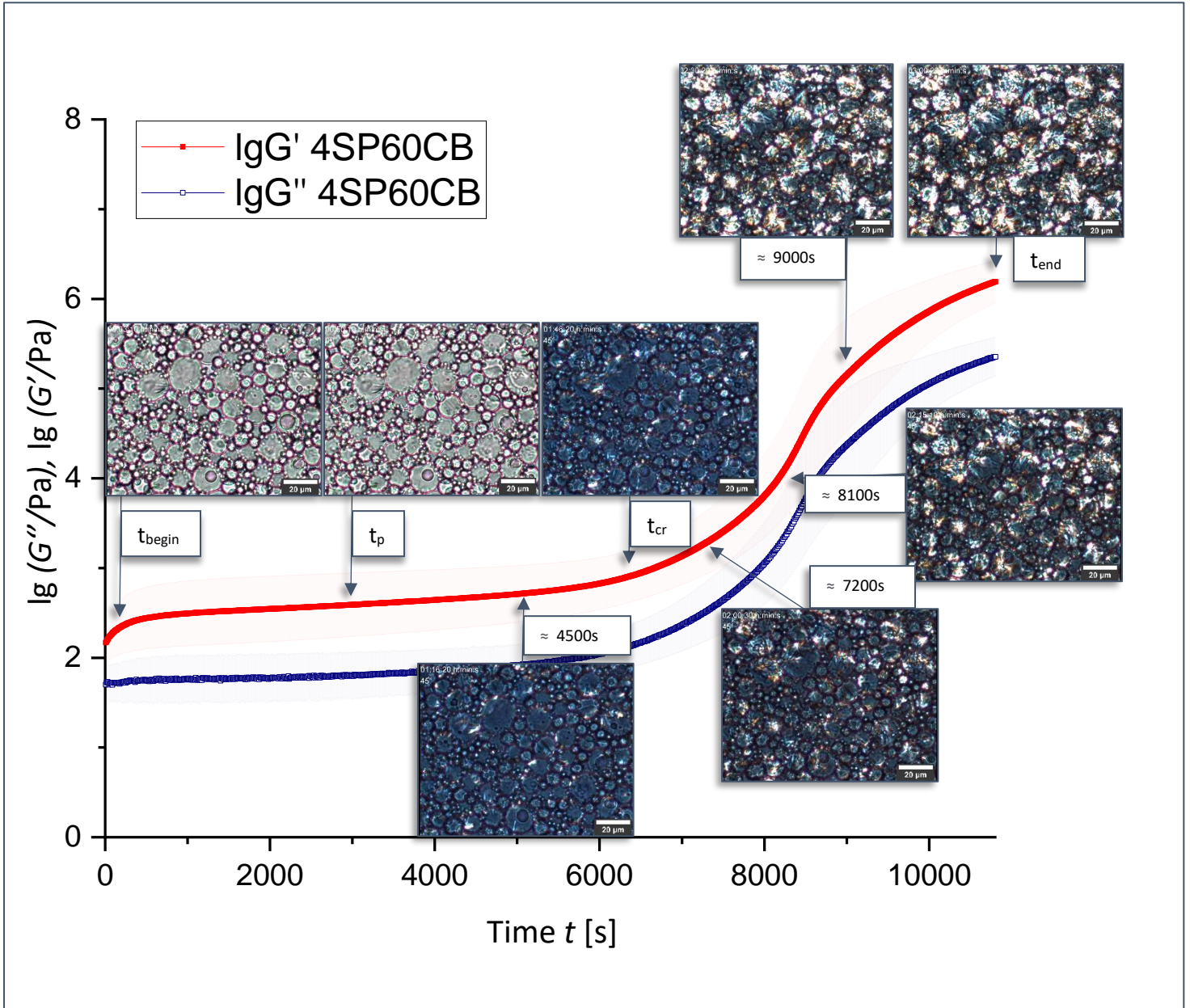


Figure 40: time-dependent rheological measurement, displaying the storage modulus G' and the loss modulus G'' of a 4SP60CB emulsion complimented by microscope pictures taken separately during the same time frame, showing the change in emulsion over time. t_{begin} \approx measurement start, $t_p \approx 3000s$, $t_{cr} \approx$ begin of rapid crystallization, $t_{end} \approx$ end of measurement.

moduli. The amount of crystals rapidly increased, as seen by the increased number of bright spots in the microscope pictures at approximately 7200 s and 8100 s. They appeared mainly in neighborhood to already formed crystals in other droplets, suggesting a secondary crystallization process, accomplished through fat crystals penetrating into other droplets, also promoting partial coalescence. With increasing SFC the crystallization process started to slow down at about 9000 s, with mainly small droplets being still liquid. Although they started to show crystallization at the end of the measurement t_{end} .

The moduli will probably still continue to slightly rise, while completing the crystallization and polymorph changes might further change the moduli. However, to prove this hypothesis, longer time measurements need to be carried out. Under the microscope a phase inversion could be observed. The individual droplets

can still be differentiated, although not as clearly anymore, hinting for partial coalescence. The original continuous water phase was pushed aside, accumulating at some places (see red frames in Figure 41, while the droplets continue to merge together (see outside of red frames in Figure 41), trapping the water phase, probably also pushing the SP aside. The SPs are likely to be expelled from the crystallizing oil phase, as their lipophilic parts would disrupt the crystal formation.

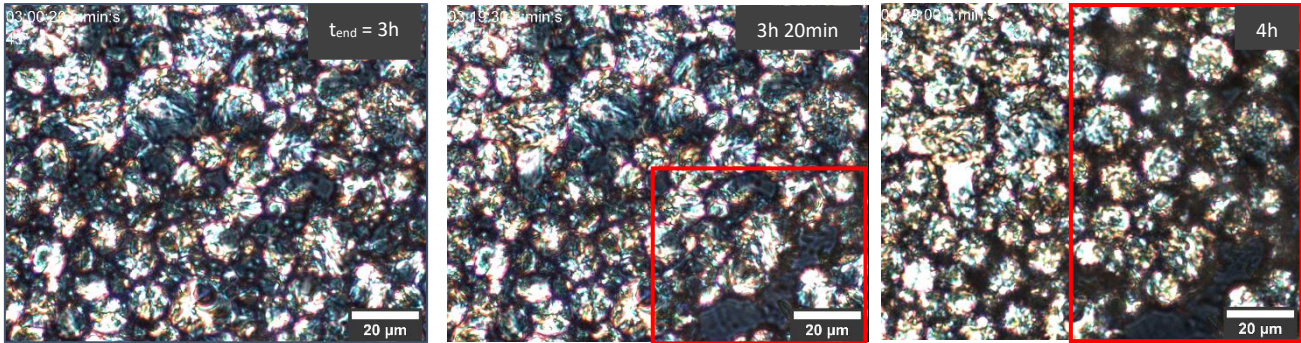


Figure 41: Microscope pictures of 4SP60CB-emulsion taken at 100x magnification, red frames: Accumulation of the watery phase. Outside of red frames partial coalescence can be seen.

The occurrence of partial coalescence was also supported through the observation of the melting behavior of an emulsion where some droplets were already crystallized and others were not, see Figure 42 (upper). This for one depends on if a droplet contains a seed crystal or not or if crystallization is induced through foreign influences such as air bubbles, invoking the growth of further crystals. These geometrical irregular shaped primary particles form with increasing amount a network (Joshi, 2018 & 2020), as it was shown in Figure 24. At first this network is restrained to the geometry of the droplet but will, with rising solid-fat-content, penetrate the surrounding protective protein layer, inducing crystallization in neighboring droplets. As seen in Figure 42 (upper), not all neighboring droplets are crystallized, hinting for one to

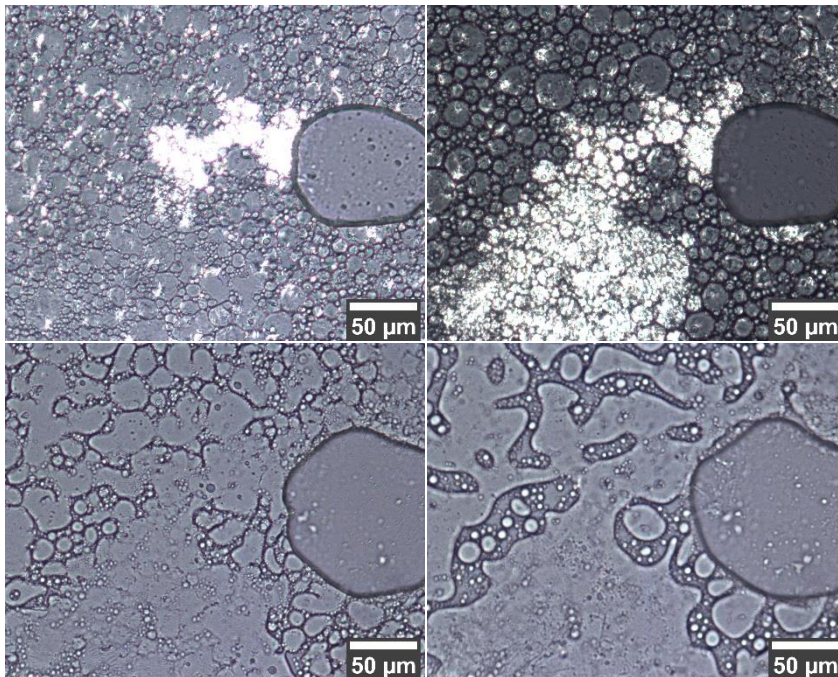


Figure 42: Crystallization at 22°C (upper pictures), followed by a temperature ramp up to 40°C (lower pictures). Effect of partial coalescence on melting behavior.

asymmetric crystal network formation and varying thickness of the protein layer. Also due to the formed crystals the droplets do not seem to keep their spherical form only partially retaining it. The partially crystallized emulsion was heated to 40°C, see Figure 42 (lower). The area with the crystallized droplets in close neighborhood to each other, did not retain any individual droplets, while droplets which were still mainly liquid, were able to retain for some time some of their shapes, before merging together when molten. As the SP was probably pushed aside during the crystallization process, with the hydrophobic side chains of the amino acids being expelled from the crystals, the soy protein would not have enough time to adsorb on the droplet surfaces again, especially since the droplets are merged, changing the existing surface availability and probably surface structure through the irregular formed crystals.

4.4.1 Crystallization Under Different Circumstances

4.4.1.1 Influence of Temperature

The influence of the temperature on the crystallization was observed. Interesting is the difference in curve shape between measurements taken at 4 °C and 22 °C, see Figure 43. The shape of the 4 °C-curve suggests that the crystallization starts right away, continually increasing the moduli, while emulsions crystallizing at 22°C show a low gradient linear area, before crystallizing rapidly. Similar curve progressions for similar

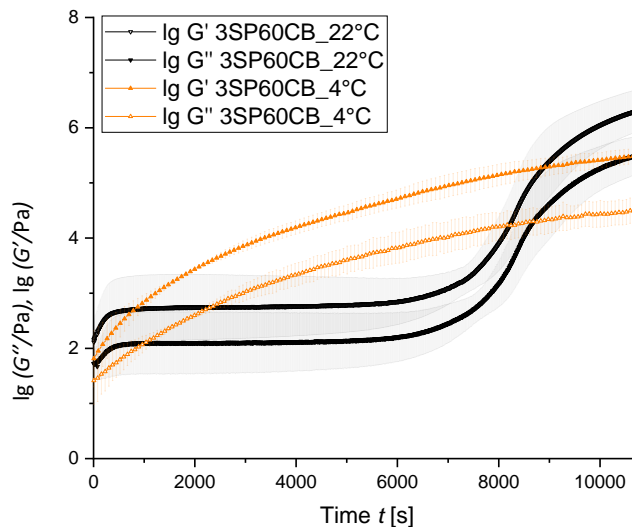


Figure 43: Time-dependent measurement of 3SP60CB measured at 4 °C and 22 °C.

temperatures were observed through determining the SFC through NMR by Di Bari et al. (2017) for water-in-cocoa butter emulsions. This suggests that the overall curve progression is at least somewhat independent of the emulsion being a W/O or O/W-emulsion.

A possible reason why the crystallization starts right away for $T = 4\text{ °C}$ and not for $T = 22\text{ °C}$ could lie for one in the degree of supercooling $\Delta T_s = T_m - T$. Cocoa butter has a melting temperatures T_m from 13 °C to 37°C, depending on the formed polymorph (see chapter 2.1). As such the degree of supercooling is of a greater magnitude for 4 °C and the critical radius needed to form a stable nucleus is much smaller, allowing for faster crystallization, than for 22°C which is in the melting range. Smaller crystals would also allow a more flexible crystal network, being one explanation for the lower moduli of the 4 °C

measurements. Another reason for the difference is the formation of different kind of polymorphs, as they are influenced by the cool down rate and crystallizing temperature (Garti & Aserin, 2012; Sasaki et al., 2012). In Figure 3: When cacao butter is cooled 'statically' at certain temperatures different crystal forms are adapted and change with time (Vilgis, 2015). It is shown that when cacao butter is cooled 'statically' at certain temperatures different crystal polymorphs are adapted, which change with time. At 4 °C it predicts the immediate formation of γ - polymorphs, followed by the formation of α - polymorphs. This corresponds with the immediate rise of moduli. At 22 °C on the other hand, it predicts no polymorph formation until about 1 h, with maybe some α -polymorphs forming in advance of β' – polymorphs. This is seen in the time-dependent measurement of the 22 °C with the low gradient linear area before the rapid rise of moduli. Another reason might be that seed crystals start to catalyze the crystallization through secondary heterogeneous nucleation below 14 °C. This primary crystallization process, promotes secondary crystallization, which accelerates the overall crystallization.(Hindle et al., 2000)

The existence of the low gradient linear area when measured at 22 °C, where the material state does not greatly change over a longer period of time, as seen in Figure 40 and Figure 43, allows for processing and enables measurements to be done in this time frame. This knowledge was used for the viscosity measurements.

4.4.1.2 Influence of Droplet Size

Emulsions prepared with different emulsifier concentrations were measured at 22 °C. For a better visibility and because there is so crossing point between the storage and the loss modulus (see appendix Figure 51), only the storage modulus is displayed (Figure 44). A graph with the included loss modulus can be found in the appendix. All four emulsion types show the already discussed curve progression with a low gradient linear range before rapidly crystallizing.

A linear fit was fitted in a suitable interval of the low gradient linear range of the single measurements to determine the average starting point of rapid crystallization t_{cr} for each sample, see Figure 50-53 in the

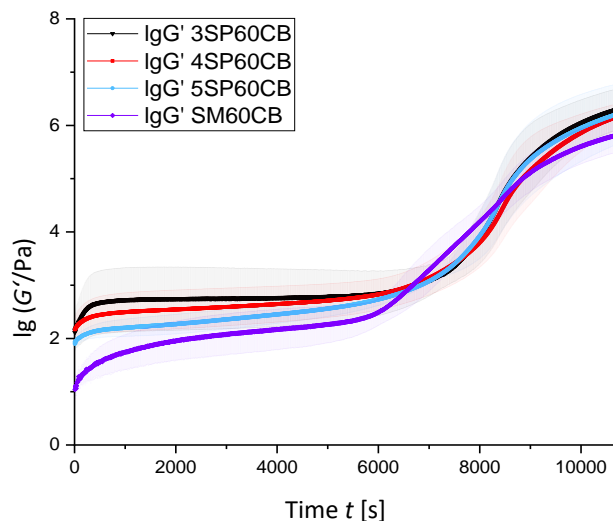


Figure 44: Time-dependent measurement of storage modulus of emulsions prepared with different SP-concentrations.

appendix. The first value deviating from linear fit by 5 % was determined as starting point of the rapid

curing process, also corresponding to the microscope timelapse. The value calculated is only an estimate giving the rough time at which the emulsion will start to rapidly change their structure, which starts at ~ 6300 s for cocoa butter emulsions stabilized with soy protein and ~ 6000 s for the sample prepared with soy milk, as shown in Table 6. Latter show the largest standard deviation from its average, probably related to the fact that those samples were not really emulsified and as such can not really crystallize with a secondary crystallisation process. The large error bars seen in Figure 44 show that the moduli for each sample of the same type is quite different, probably depending on the from the in the beginning contained crystals. All three sample types prepared with SP display a similar rapid crystallisation rate, as seen from the similar gradients in the Interval between 7700 s and 8700 s, see Table 6.

Table 6: Determined starting point of curing t_{cr} and crystallization rate, signified through the rise of the storage modulus in time, the gradient m .

	t_{cr} [s]	Δt_{cr} [s]	Gradient m [Pa/s]	Δm [Pa/s]
			Interval: 7700s - 8700s	
3SP60CB	6313	± 628	1.5E-03	1.3E-05
4SP60CB	6327	± 285	1.3E-03	1.7E-05
5SP60CB	6293	± 339	1.5E-03	1.4E-05
SM60CB	5954	± 738	9.6E-04	2.4E-06

The low gradient linear range on the other hand diverges for each sample. While 3SP60CB shows a plateau-like linear area, the 4SP60CB- and 5SP60CB-emulsion show monotonous rising from the beginning. This might also be influenced by the fact that the droplets, as they are smaller, are packed closer together, promoting secondary crystallization, as it is easier for fat crystals to penetrate neighboring droplets in closer proximity, due to a significantly larger gain of energy. Also some crystals might have already started to form. Especially the beginning is strongly dependent on the sample history, the time needed to start the measurement and surrounding temperature, as well as already contained crystal seeds. There might be a correlation to the particle size, but to confirm this, more measurements need to be performed.

The measurements of the SM-samples on the other hand behave differently. This was to be expected as they were not emulsified completely, as shown before in Figure 37. Also SM contains not only SP but also other materials of the soybean, which could also influence the crystallization, as the emulsifier layer around contained droplets might be of a different composition or thickness, influencing the secondary crystallization process. The crystallization starts in general earlier, also the storage modulus increases at a slower rate than the SP-emulsions, see Table 6. This might be because it is more similar to bulk material, needing less nuclei as there are less SP-barriers preventing the spreading of the crystals. At the beginning all emulsion types show different loss factors $\tan \delta$, but still indicating viscoelastic solid like behavior, with the SM-sample showing the most fluid like behavior. This is probably because of the large areas of liquid fat, behaving more similar to an ideal liquid than the droplet dominated SP-Emulsions.

Table 7: Loss factor $\tan \delta$ at different time points in the crystallization process.

	$\tan \delta_{\text{begin}}$ t=8s	$\Delta \tan \delta_{\text{begin}}$	$\tan \delta_{\text{plateau}}$ t=3000s	$\Delta \tan \delta_{\text{plateau}}$	$\tan \delta_{\text{cr}}$ t=t _{cr}	$\Delta \tan \delta_{\text{cr}}$	$\tan \delta_{\text{end}}$ t=10801s	$\Delta \tan \delta_{\text{end}}$
3SP60CB	0.47	± 0.13	0.25	± 0.04	0.22	± 0.03	0.16	± 0.01
4SP60CB	0.39	± 0.12	0.19	± 0.04	0.20	± 0.02	0.15	± 0.01
5SP60CB	0.40	± 0.02	0.23	± 0.02	0.20	± 0.01	0.15	± 0.01
SM60CB	0.63	± 0.13	0.26	± 0.06	0.20	± 0.05	0.16	± 0.01

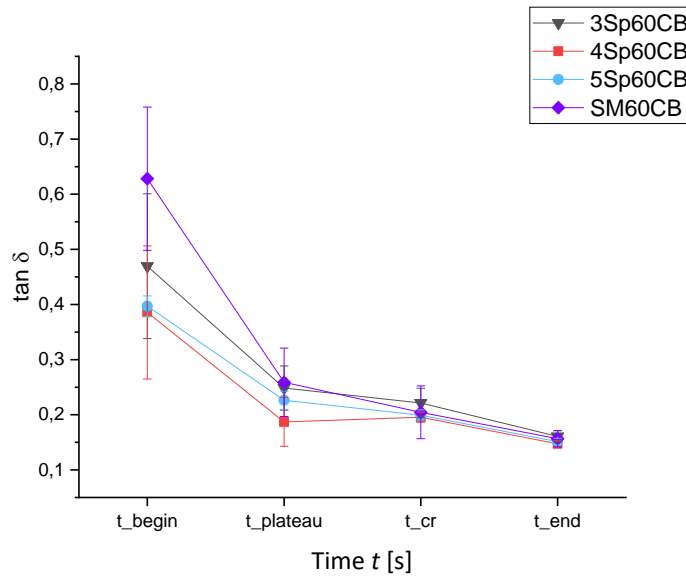


Figure 45: Loss factor $\tan \delta$ of time-dependent measurement at different time points in the crystallization process.

The value of $\tan \delta$ then rapidly falls, see Figure 45. But independently of how their crystallization progressed, in the end all four emulsion types show similar values of $\tan \delta_{\text{end}} = 0.16 \pm 0.01$, shown in Table 7.

The decrease of $\tan \delta$ shows an increase in viscoelastic solid properties, see Table 3, indicating that the end rheological behavior is more dominated through the established fat crystal network, than the droplet size, further supporting the hypothesis about partial coalescence.

Similarly, the rheology of water-in-oil emulsions, such as margarine or butter, is largely determined by the rheological characteristics of the fat crystal network present in the oil phase (Marangoni & Weddorp, 2012)

4.5 Behavior of Crystallized Emulsions

4.5.1 Network Occurrence

To gain a deeper understanding of the structure after crystallization a frequency sweep was performed. All samples show a similar curve progression with an increasing storage modulus G' and a decreasing loss modulus G'' with rising frequency, while $G' > G''$, shows viscoelastic solid like behavior throughout each measurement, see Figure 46.

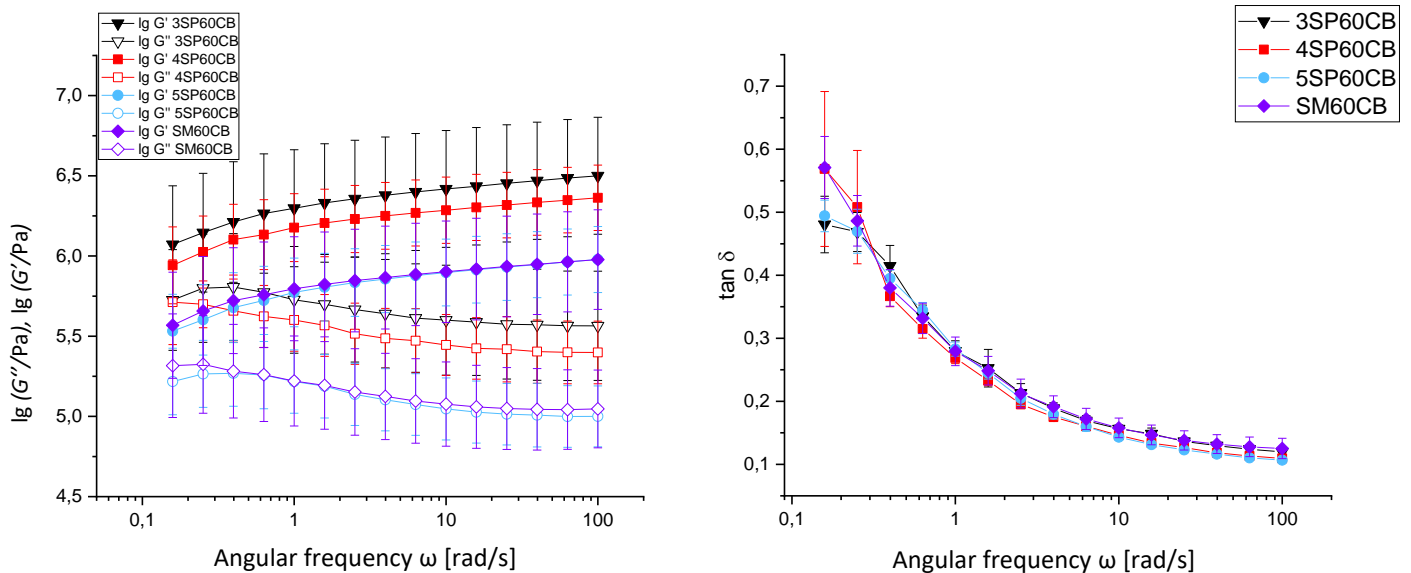


Figure 46: Frequency sweep of the different emulsion types; left: Storage and loss modulus, right: loss factor $\tan \delta$ at different frequencies.

This kind of curve progression was also observed by Narine & Marangoni (1999) for non-emulsified CB. They proposed that the ratio of G''/G' , the $\tan \delta$, is linked to the microstructure of the CB. As mentioned in chapter 2.1, the TAGs of the CB form highly ordered crystal lattices upon crystallization. A three-dimensional network is formed, as the crystals aggregate, forming a fractal lattice. Through partial coalescence this network spreads throughout the whole emulsion. As seen in Figure 36 (right) the $\tan \delta$ is very similar between the different emulsions types, independent of their droplet size, only slightly differentiating at low frequencies. At low frequencies, the relative movement between the crystals would not be as restricted, as the network would be able to adjust flexible in time with the shear, showing more viscous behavior with a higher loss modulus. With higher frequencies the network becomes more inflexible, as shown through the decreasing $\tan \delta$, see Figure 46 (right), because the network is able to store more energy through the rising restriction of the relative movements between the crystals. This can also be seen through the rising storage modulus.

It is interesting to see that the storage and loss modulus of SM60CB and 5SP60CB overlap, in contrast to the moduli from 4SP60CB and 3SP60CB, which are at higher values, thus increasing with decreasing SP-content. It is most likely that this is because the droplets of 5SP60CB are smaller and thus closer packed, behaving more similar to the bulklike SM60CB when crystallized.

4.5.2 Network Stability

To observe the network stability of the crystalized emulsion, a controlled shear deformation (CSD)-test, also called amplitude sweep was performed. As seen in Figure 47 (left), all samples show a similar curve progression.

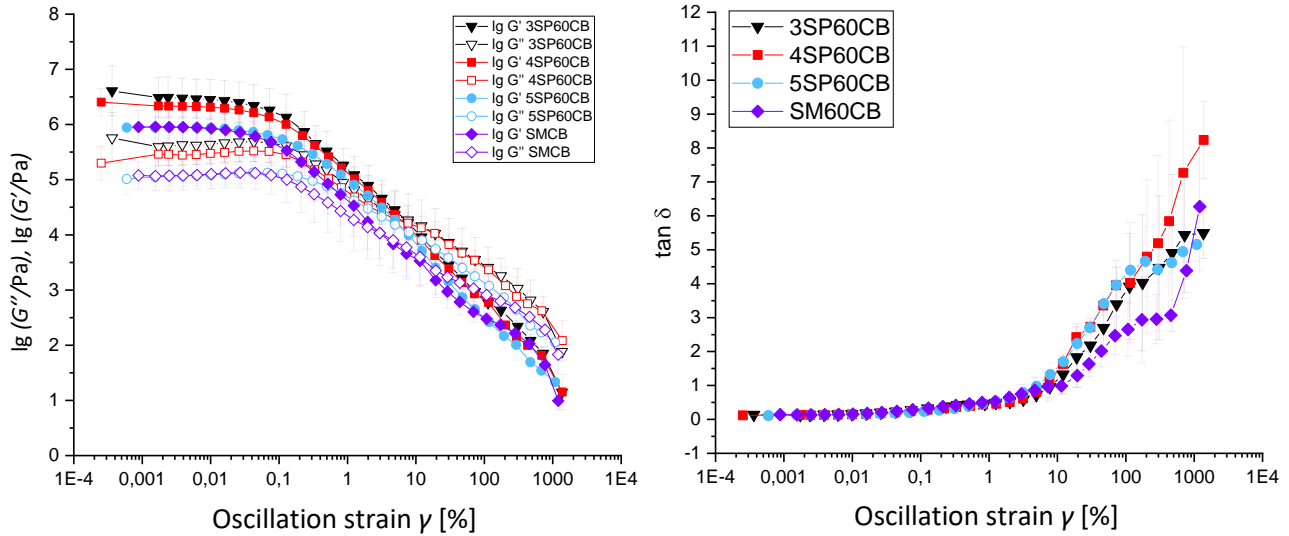


Figure 47: Amplitude sweep of the different emulsion types; left: Storage and loss modulus, right: loss factor $\tan \delta$ at different γ .

In the LVE-range the storage modulus G' has higher values than the loss modulus G'' , the elastic behavior dominates over the viscous behavior, indicating a certain degree of stiffness of the system. In the microscope pictures it was observed how the fat crystallizes, also connecting the individual droplets through fat crystal “bridges”, partially merging them, which is a possible explanation for the indicated stiffness. In the LVE-range the CB crystal structure does not show any significant changes, which was why 0.01 % was chosen for the before mentioned experiments (time and frequency sweep). A certain deformation threshold needs to be surpassed to irreversibly change the crystal lattice. This yield point γ_L can be defined as the strain at which the storage modulus deviates by 5 % from the value of the LVE-range. The determined yield points were only slightly above $\gamma = 0.1$ %, indicating a very inflexible structure (Mezger, 2016). For 3SP60CB and 4SP60CB the yield points were in the same range, see Table 8, while for 5SP60CB it is at higher values and the one for SM60CB is lower values. Considering the error values the difference is not that significant, although emulsified CB seems to show irreversible structure changes later, maybe because the trapped water droplets in the network structure allow for a greater flexibility of the network.

Table 8: Yield points γ_L , flow points γ_F and flow-transition index γ_L/γ_F of the different emulsion types.

	γ_L [%]	$\Delta \gamma_L$ [%]	γ_F [%]	$\Delta \gamma_F$ [%]	γ_L/γ_F	$\Delta \gamma_L/\gamma_F$
3SP60CB	0.18	± 0.05	6.3	± 1.4	35.0	± 12.5
4SP60CB	0.18	± 0.05	6.3	± 1.4	35.0	± 12.5
5SP60CB	0.25	± 0.06	6.5	± 1.5	25.8	± 8.5
SM60CB	0.11	± 0.03	3.9	± 0.9	36.7	± 11.9

A slight rise of the loss modulus G'' can be observed before it steadily decreases, showing the existence of a network structure of the CB crystals, further supporting the occurrence of partial coalescence. It is only a slight rise as the CB crystals are not chemically connected, but rather form a network because of stacking compatibility and aggregation of crystallites to primary particles, which further aggregating together to form a network. The rising values of G'' hint to a rising amount of deformation energy used up before the final breakdown of the internal structure. Some areas of the network might already irreversibly deform, with for example micro cracks appearing. The links between the blobs mentioned in chapter 2.4.3 start to break. These enable relative movements between the network fractions, consuming energy through internal friction, seen with the loss modulus. When the micro cracks grow to the macroscale the sample will start to flow, seen as the flow point γ_f where $G' = G''$. At this point even the bonds inside the blobs break, separating the primary particles. SM60CB seems to start to flow earlier than



Figure 49: Sample after amplitude test.

the better emulsified samples, see flow points γ_f in table. Until the flow point, all samples show a similar viscoelastic behavior, with the curve progression of the individual $\tan \delta < 1$ overlapping. As soon as $\tan \delta > 1$, with the viscous behavior now dominating, all samples show very different curve progressions, which are not reliable. The sample, as seen in Figure 49, was apparently not sheared homogeneously anymore, taking on wormlike appearances at the end of the amplitude sweep, with the original macroscopic structure destroyed. The worms also allowed for more energy to be lost through friction than to be stored. As such the flow point might indicate, when the first “worms” started appearing. Although the error is quite large, the flow transition index is above one, showing that the network structure is not entirely brittle and does not break apart immediately upon reaching the yield point. Especially since the fat network is not formed uniformly, linking some blobs more often than others, forming a highly complex, heterogeneous crystal system. The growth direction of this network might have been influenced by the soy protein, but as they are dispelled from the solid crystals, their influence on the deformation behavior of the emulsion decreases. Emulsion droplets could be seen as blobs on a larger scale, linked to other

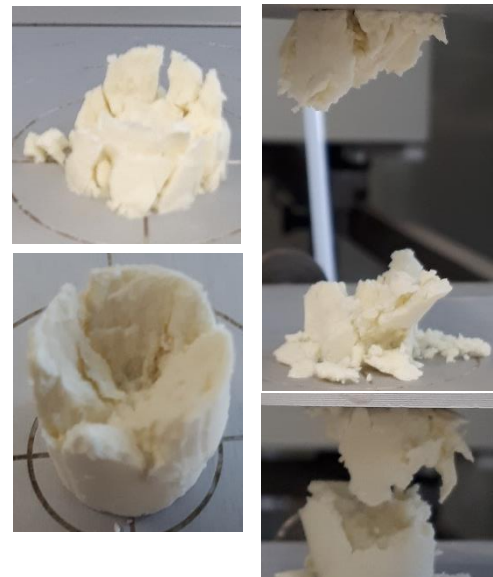
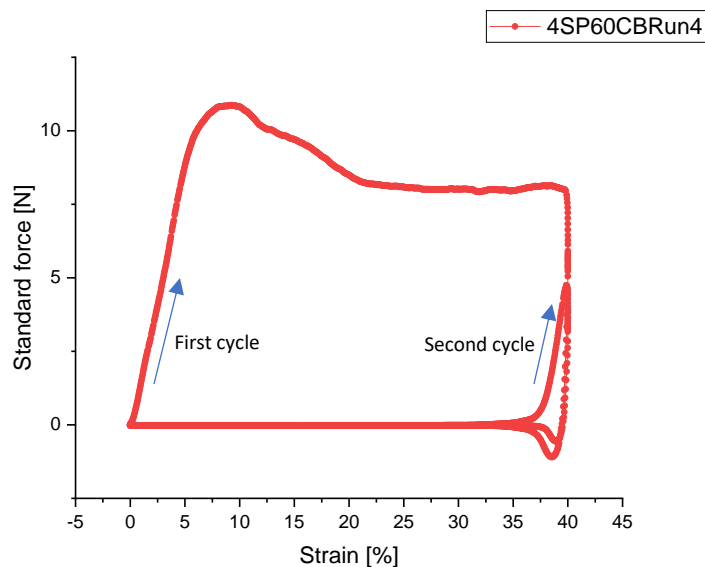


Figure 48: left: graphical display of pressure experiment, strain = percentage of sample height. right: Random breaking behavior of emulsion samples.

blobs (droplets) by the bridges created by partial coalescence. The systems probably start to first form micro cracks in the areas where the droplets are not that well connected, in the areas with the accumulated soy protein water phase. The heterogeneity of the network was also observed by the not uniformly appearing of cracks when pressure was applied to a cylindrical molded one day old sample, see Figure 48 (right).

As the cracks appeared randomly, no reproducible measurements were obtained, although the general shape of the graphs of each measurement was quite similar, with first a rapid rise of the standard force, followed by a slight decreases and a plateau, see Figure 48 (left). The maximum is the point at which the sample stops deforming and starts to break apart. The late appearance of the second circle shows that the sample did not flow, but remained partially solid, being deformed again, when, during the second cycle, the broken parts touched each other again.

5 Summary

In summary protein stabilized cocoa butter-emulsions are excellent examples to explore general theories about crystalizing emulsions. In the beginning it was shown that a certain amount of mechanical energy is needed to produce a kinetical stable emulsion, and the emulsion cannot be simply diluted with water but needs additional surfactants (here 1% SDS-Solution and 60mmol NaCl was used) to ensure spherical droplets and avoid agglomerations. The packing behavior of polydisperse emulsions with up to $\phi = 75$ wt% oil-content could be observed with the help of polarized light microscopy, allowing the application of concentrated system models. For further observation, an emulsion showcasing a glassy system with $\phi = 60$ wt% was chosen. Viscosity measurements showing shear thinning behavior, matched the assumption of a glassy system, as well is a typical behavior for emulsions. Smaller droplets and emulsion compared to the sole continuous phase, the soy protein dispersion, displayed higher viscosity values. With the SP the droplet size distribution is easier to control than with soy milk, which protein content depends on season and origin of the soybean and thus did not show uniform emulsification capabilities. The droplet size decreases with higher emulsifier content, as it is able to cover more surface area. Regarding the final rheological behavior, the droplet size does not make that much of a difference. A fat-crystallizing induced phase inversion was observed. Emulsions change over time through fat-crystallization from a liquid O/W-emulsion to a solid W/O-emulsion. The main crystallization started, depending on the temperature, either right away or after a period of about one and a half hour. The crystallization occurred probably through secondary heterogeneous nucleation, initiating a secondary crystallization process. Partial coalescence, the cause for the phase inversion, was observed in microscope pictures. Because of partial coalescence crystallized emulsions are even less stable upon heating, as the stabilizing proteins were probably pushed aside during the partial merging of the droplets and are not able to restabilize the system upon returning the droplets to their liquid state. The effect of partial coalescence on the structure was possible to be observed through a frequency test, suggesting the appearance of a superordinate network, a three-dimensional crystal network. As such there was not a big difference between the emulsions, as the network was formed throughout the whole system, connecting the droplets not isolating them. A loss factor of $\tan \delta \approx 0.16 \pm 0.01$ was similar for all samples, describing a viscoelastic solid. The network also influenced the stiffness if the emulsion making them quite brittle. Regarding the soy milk and pure soy protein dispersion, there were differences between those two, but only slightly diverging ones, such as a lower storage and loss modulus. This is probably due to the fact that soy milk also contains other substances aside from soy protein. In conclusion it can be said that more similar results are achievable through the usage of soy protein, but for everyday use in the kitchen, soy milk would be enough, as the end results do not differ much. The values of the measurement cannot be directly applied to chocolate systems as in chocolate suspended materials will change the rheological behavior, but it is still usable to transfer basic knowledge of the processes happening.

6 Outlook

The methods used in this thesis allowed to gain a fundamental understanding over the processes and properties occurring in a cocoa butter emulsion stabilized with soy protein and might even allow to transfer some knowledge gained here to other crystallizing emulsions.

But to gain a better insight of, for example, the crystal network formed in this emulsion system and its effect on the brittleness of the samples, it would be interesting to use differential scanning calorimetry (DSC) to determine the polymorphs formed during the crystallization in the soy protein stabilized cocoa butter emulsions. Depending on the kind of polymorph formed, crystallized samples will be softer or harder and will taste differently. This also depends on the cooling rate. With this technique it would also be possible to determine if the soy proteins are denatured or not, enabling a better understanding of how the proteins are adsorbed to the interface of the phases.

Determining the SFC or amount of crystal seeds directly after preparing the emulsion might help to understand the influences of already contained crystals and primary crystallization on secondary crystallization. It might even be possible to determine the timepoint of phase inversion through performance of electronic conductivity tests, as it should change greatly depending on the continuous phase.

With nuclear magnetic resonance (NMR) the droplet size distribution of the water droplets formed during the phase inversion could be determined and would give a better understanding of the long-term stability of the system.

Measuring the zeta potential of the emulsion, would further support the findings of the droplet size distribution of rising emulsifier content lowering the droplet size, as the zeta potential measures the surface potential of a droplet. This value depends on the droplet size, as the droplet size is dependent on the surface tension. Also it would be possible to gain a better understanding of the repulsive or attractive interaction of the soy protein, which are directly related to agglomeration formation of emulsion droplets. There are many more possibilities, not only with the above mentioned methods, but also with different settings of the in this thesis presented methods. As such it is possible to say that there is still a lot more to learn about this system.

Literature

- Abramov, S., Ruppik, P., & Schuchmann, H. P. (2016). Crystallization in emulsions: A thermo-optical method to determine single crystallization events in droplet clusters. *Processes*, 4(3). <https://doi.org/10.3390/pr4030025>
- Allouche, J., Tyrode, E., Sadtler, V., Choplin, L., & Salager, J. L. (2004). Simultaneous Conductivity and Viscosity Measurements as a Technique To Track Emulsion Inversion by the Phase-Inversion-Temperature Method. *Langmuir*, 20(6), 2134–2140. <https://doi.org/10.1021/la035334r>
- Belitz, H.-D., Grosch, W., & Schieberle, P. (2008). *Lebensmittelchemie* (6.), Springer.
- Beverung, C. J., Radke, C. J., & Blanch, H. W. (1999). Protein adsorption at the oil/water interface: Characterization of adsorption kinetics by dynamic interfacial tension measurements. *Biophysical Chemistry*, 81(1), 59–80. [https://doi.org/10.1016/S0301-4622\(99\)00082-4](https://doi.org/10.1016/S0301-4622(99)00082-4)
- Chapman, G. M., Akehurst, E. E., & Wright, W. B. (1971). Cocoa butter and confectionery fats. Studies using programmed temperature X-ray diffraction and differential scanning calorimetry. *Journal of the American Oil Chemists Society*, 48(12), 824–830. <https://doi.org/10.1007/BF02609292>
- Davis, T.R., & Dimick, P. S. (1986). Solidification of Cocoa Butter. *Proc. PMCA Prod. Conf.*, 40, 104–108.
- Davis, Thomas R., & Dimick, P. S. (1989). Lipid composition of high-melting seed crystals formed during cocoa butter solidification. *Journal of the American Oil Chemists' Society*, 66(10), 1494–1498. <https://doi.org/10.1007/BF02661979>
- Derkach, S. R. (2009). Rheology of emulsions. *Advances in Colloid and Interface Science*, 151(1–2), 1–23. <https://doi.org/10.1016/j.cis.2009.07.001>
- Di Bari, V., Macnaughtan, W., Norton, J., Sullo, A., & Norton, I. (2017). Crystallisation in water-in-cocoa butter emulsions: Role of the dispersed phase on fat crystallisation and polymorphic transition. *Food Structure*, 12, 82–93. <https://doi.org/10.1016/j.foostr.2016.10.001>
- Duck, W. (1964). The Measurement of Unstable Fat in Finished Chocolate. *Manufacturing Confectioner*, 35(6), 67–72.
- EUROSOY GmbH. (2019). *Vegacon*® 90 (Issue March).
- Fredrick, E., Walstra, P., & Dewettinck, K. (2010). Factors governing partial coalescence in oil-in-water emulsions. *Advances in Colloid and Interface Science*, 153(1–2), 30–42. <https://doi.org/10.1016/j.cis.2009.10.003>
- Garti, N., & Aserin, A. (2012). Effect of Emulsifiers on Cocoa Butter and Chocolate Rheology, Polymorphism, and Bloom. In N. Garti & N. R. Widlak (Eds.), *Cocoa Butter and Related Compounds* (pp. 275–305). Elsevier. <https://doi.org/10.1016/B978-0-9830791-2-5.50015-3>
- Ghazani, S. M., & Marangoni, A. G. (2019). The Ternary Solid State Phase Behavior of Triclinic POP, POS, and SOS and Its Relationship to CB and CBE Properties. *Crystal Growth and Design*, 19(2), 704–713. <https://doi.org/10.1021/acs.cgd.8b01273>
- Gompper, G., Dhont, J. K. G., & Richter, D. (2003). Komplexe Materialien auf mesoskopischer Skala: Was ist Weiche Materie? *Physik in Unserer Zeit*, 34(1), 12–18. <https://doi.org/10.1002/piuz.200390002>
- Hindle, S., Povey, M. J. W., & Smith, K. (2000). Kinetics of crystallization in n-hexadecane and cocoa butter

- oil-in-water emulsions accounting for droplet collision-mediated nucleation. *Journal of Colloid and Interface Science*, 232(2), 370–380. <https://doi.org/10.1006/jcis.2000.7174>
- Huyghebaert, A., & H. Hendrickx. (1971). Polymorphism of Cocoa Butter, Shown by Differential Scanning Calorimetry. *Lebensm. Wiss. Technol.*, 4(2), 59–63.
- IKA® WERKE. (2006). IKA® WERKE IKA ULTRA-TURRAX® T 18 basic. IKA® WERKE.
- Jiang, S., Cai, W., & Xu, B. (2013). Food Quality Improvement of Soy Milk Made from Short-Time Germinated Soybeans. *Foods*, 2(2), 198–212. <https://doi.org/10.3390/foods2020198>
- Joshi, B., Beccard, S., & Vilgis, T. A. (2018). Fractals in crystallizing food systems. *Current Opinion in Food Science*, 21, 39–45. <https://doi.org/10.1016/j.cofs.2018.05.009>
- Joshi, B. L., Zielbauer, B. I., Vilgis, T. A. (2020). Comparative Study on Mixing Behavior of Binary Mixtures of Cocoa Butter/Tristearin (CB/TS) and Cocoa Butter/Coconut Oil (CB/CO). *Foods*, 9(3), 327. <https://doi.org/10.3390/foods9030327>
- Landfeld, A., Novotna, P., Strohalm, J., Houska, M., & Kyhos, K. (2000). Viscosity of cocoa butter. *International Journal of Food Properties*, 3(1), 165–169. <https://doi.org/10.1080/10942910009524623>
- Lipp, M., Simoneau, C., Ulberth, F., Anklam, E., Crews, C., Brereton, P., De Greyt, W., Schwack, W., & Wiedmaier, C. (2001). Composition of genuine cocoa butter and cocoa butter equivalents. *Journal of Food Composition and Analysis*, 14(4), 399–408. <https://doi.org/10.1006/jfca.2000.0984>
- Liu, P., Xu, H., Zhao, Y., & Yang, Y. (2017). Rheological properties of soy protein isolate solution for fibers and films. *Food Hydrocolloids*, 64, 149–156. <https://doi.org/10.1016/j.foodhyd.2016.11.001>
- Loisel, C., Keller, G., Lecq, G., Bourgaux, C., & Ollivon, M. (1998). *Phase Transition and Polymorphism of Cocoa butter*. 75(4), 425–439.
- Lonchampt, P., & Hartel, R. W. (2004). Fat bloom in chocolate and compound coatings. *European Journal of Lipid Science and Technology*, 106(4), 241–274. <https://doi.org/10.1002/ejlt.200400938>
- Lovegren, N. V., Gray, M. S., & Feuge, R. O. (1976). Polymorphic changes in mixtures of confectionery fats. *Journal of the American Oil Chemists' Society*, 53(2), 83–88. <https://doi.org/10.1007/BF02637399>
- Marangoni, A. G., & Wesdorp, L. H. (2012). *Structure and properties of fat crystal networks* (2nd ed.). CRC Press.
- McClements, D. J. (2010). *Food Emulsions Principles, Practices, and Techniques* (3rd ed.). CRC Press. <https://doi.org/10.1201/9781420029581.ch9>
- McClements, D. J. (2012). Crystals and crystallization in oil-in-water emulsions: Implications for emulsion-based delivery systems. *Advances in Colloid and Interface Science*, 174, 1–30. <https://doi.org/10.1016/j.cis.2012.03.002>
- McNaught, A., & Wilkinson, A. D. (Eds.). (2009). *IUPAC Compendium of Chemical Terminology*. IUPAC. <https://doi.org/10.1351/goldbook>
- Merken, G. V., & Vaeck, S. V. (1980). Etude du polymorphisme du beurre de cacao par calorimétrie DSC.

Lebensm. Wiss. Technol., 13, 314–317.

- Meursing, E. H. (1994). Cocoa mass, cocoa butter, cocoa powder. In S. T. Beckett (Ed.), *Industrial Chocolate Manufacture and Use* (2nd ed., pp. 70–82). Springer US. https://doi.org/10.1007/978-1-4615-2111-2_6
- Mezger, T. G. (2016). Das Rheologie Handbuch. In *Das Rheologie Handbuch Für Anwender von Rotations- und Oszillations-Rheometern* (Issue 5., p. 512). Vincentz Network. <https://doi.org/10.1515/9783748600121-009>
- Müller, M. (2012). *Emulgiertechnik: Grundlagen, Verfahren und Anwendungen* (K. Köhler & H. P. Schuchmann (Eds.)). b. Behr's Verlag GmbH & Co. KG. (Issue 3.,p.546), ISBN: 978-3-89947-869-3
- Nagano, T., Akasaka, T., & Nishinari, K. (1994). Dynamic viscoelastic properties of glycinin and β -conglycinin gels from soybeans. *Biopolymers*, 34(10), 1303–1309. <https://doi.org/10.1002/bip.360341003>
- Narine, S. S., & Marangoni, A. G. (1999). The difference between cocoa butter and salatrim[®] lies in the microstructure of the fat crystal network. *JAOCs, Journal of the American Oil Chemists' Society*, 76(1), 7–13. <https://doi.org/10.1007/s11746-999-0040-4>
- Nishinari, K., Fang, Y., Guo, S., & Phillips, G. O. (2014). Soy proteins: A review on composition, aggregation and emulsification. *Food Hydrocolloids*, 39, 301–318. <https://doi.org/10.1016/j.foodhyd.2014.01.013>
- Pearce, K. N., & Kinsella, J. E. (1978). Emulsifying Properties of Proteins: Evaluation of a Turbidimetric Technique. *Journal of Agricultural and Food Chemistry*, 26(3), 716–723. <https://doi.org/10.1021/jf60217a041>
- Saio, K., Kamiya, M., & Watanabe, T. (1969). Food processing characteristics of soybean 11s and 7s proteins. *Agricultural and Biological Chemistry*, 33(9), 1301–1308. <https://doi.org/10.1080/00021369.1969.10859465>
- Sasaki, M., Ueno, S., & Sato, K. (2012). Polymorphism and Mixing Phase Behavior of Major Triacylglycerols of Cocoa Butter. In N. Garti & N. R. Widlak (Eds.), *Cocoa Butter and Related Compounds* (Vol. 60, Issue 6, pp. 151–172). Elsevier. <https://doi.org/10.1016/B978-0-9830791-2-5.50009-8>
- Smith, A. K., Rackis, J. J., Isnardi, P., Cartter, J. L., & Krober, O. . (1996). Nitrogen Solubility Index, Isolated Protein Yield, and Whey Nitrogen Content of Several Soybean Strains. *Cereal Chem*, 43, 261–269. <https://www.cerealsgrains.org/publications/cc/backissues/1966/Documents/CC1966a24.html> [viewed on 25.07.2020]
- Souley, A., & Y, T.-A. T. (2009). Effect of Processing Methods on Quality of Soymilk. *Pakistan Journal of Nutrition*, 8(8), 1156–1158.
- Sugimoto, T., Moria, T., Mano, J., Mutoh, T. A., Shiinoki, Y., & Matsumura, Y. (2001). Effects of fat crystallization on the behavior of proteins and lipids at oil droplet surfaces. *JAOCs, Journal of the American Oil Chemists' Society*, 78(2), 183–188. <https://doi.org/10.1007/s11746-001-0241-z>
- Tang, C. H., & Liu, F. (2013). Cold, gel-like soy protein emulsions by microfluidization: Emulsion characteristics, rheological and microstructural properties, and gelling mechanism. *Food Hydrocolloids*, 30(1), 61–72. <https://doi.org/10.1016/j.foodhyd.2012.05.008>

- Thanasukarn, P., Pongsawatmanit, R., & McClements, D. J. (2004). Influence of emulsifier type on freeze-thaw stability of hydrogenated palm oil-in-water emulsions. *Food Hydrocolloids*, *18*(6), 1033–1043. <https://doi.org/10.1016/j.foodhyd.2004.04.010>
- Thanasukarn, P., Pongsawatmanit, R., & McClements, D. J. (2006). Impact of fat and water crystallization on the stability of hydrogenated palm oil-in-water emulsions stabilized by a nonionic surfactant. *Journal of Agricultural and Food Chemistry*, *54*(10), 3591–3597. <https://doi.org/10.1021/jf0524630>
- Vilgis, T. A. (2015). Soft matter food physics - The physics of food and cooking. *Reports on Progress in Physics*, *78*(12), 124602. <https://doi.org/10.1088/0034-4885/78/12/124602>
- Walstra, P. (2003). Physical Chemistry of Foods. In O. R. Fennema, Y. H. Hui, M. Karel, P. Walstra, & R. John (Eds.), *Food Chemistry* (Vol. 85, Issue 2). Marcel Dekker, Inc. [https://doi.org/10.1016/s0308-8146\(03\)00246-2](https://doi.org/10.1016/s0308-8146(03)00246-2)
- Wille, R. L., & Lutton, E. S. (1966). Polymorphism of cocoa butter. *Journal of the American Oil Chemists' Society*, *43*(8), 491–496. <https://doi.org/10.1007/BF02641273>
- Zeiss, C. (2009). *Bedienungsanleitung Axio Scope.A1 Mikroskop für Routine und Einstiegsforschung* (5th ed.). Carl Zeiss Microlmaging GmbH.
- Zhang, H., Li, L., Tatsumi, E., & Isobe, S. (2005). High-pressure treatment effects on proteins in soy milk. *LWT - Food Science and Technology*, *38*(1), 7–14. <https://doi.org/10.1016/j.lwt.2004.04.007>

Appendix

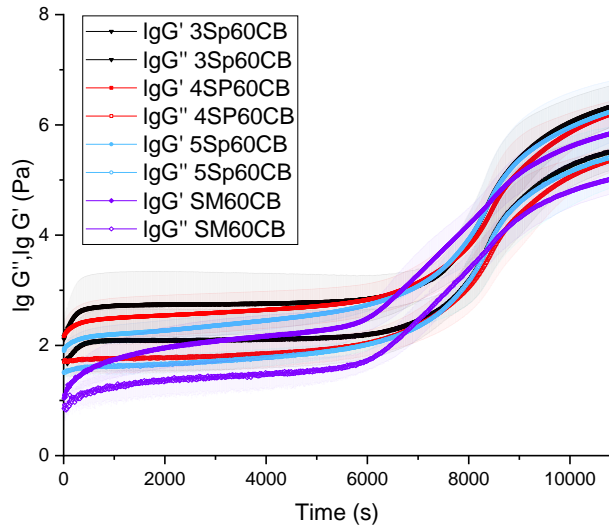
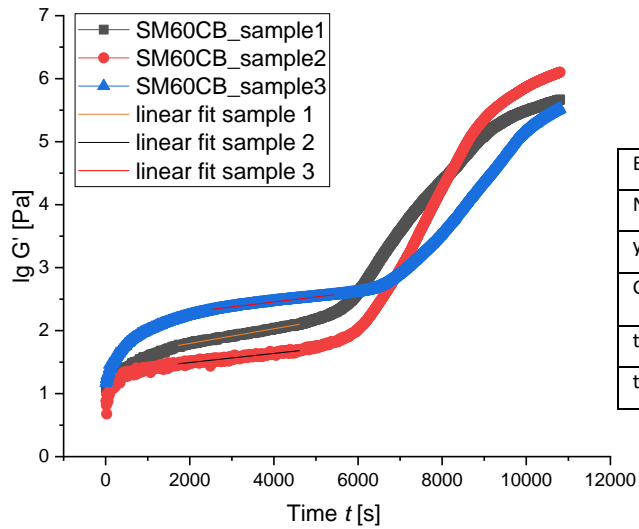
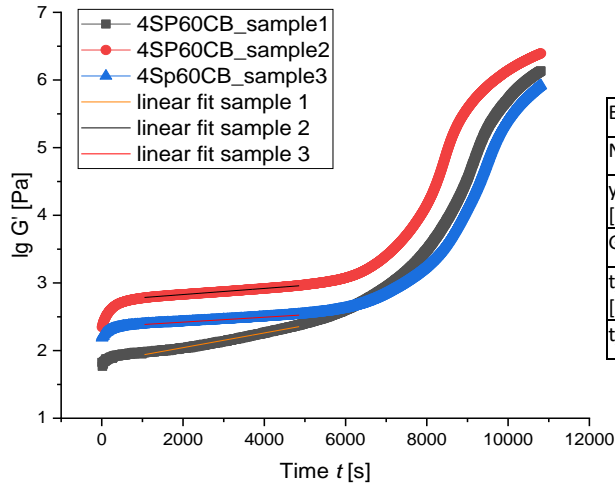


Figure 51: Time-dependent measurement of emulsions, prepared with different SP-concentrations. Upper plot of two plots of the same color is $\lg G'$, lower $\lg G''$.



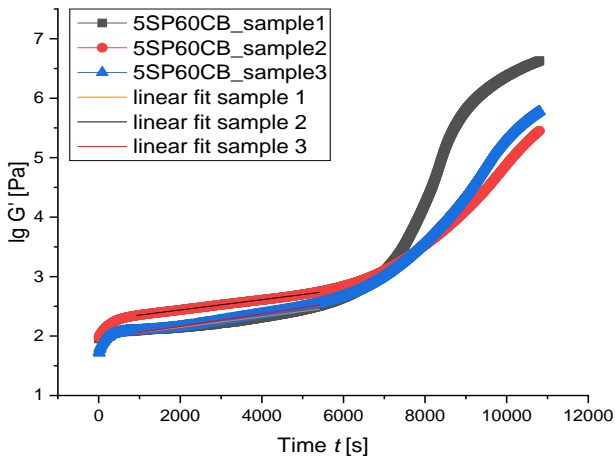
Equation	$y = a + b \cdot x$		
Name	SM60CB_sample1	SM60CB_sample2	SM60CB_sample3
y-intercept [Pa]	1.564 ± 0.001513	1.349 ± 0.003301	2.138 ± 0.001542
Gradient [Pa/s]	$1.166E-4 \pm 4.617E-7$	$7.242E-5 \pm 1.007E-6$	$7.944E-5 \pm 3.792E-7$
$t_{cr_samplex}$ [s]	$5.5204E+03$	$5.5359E+03$	$6.8063E+03$
t_{cr} [s]	$5.9542E+03 \pm 7.3799E+02$		

Figure 50: Time-dependent measurement of emulsions, prepared with Soy milk. $\lg G'$ is shown with linear fit to determine t_{cr} .



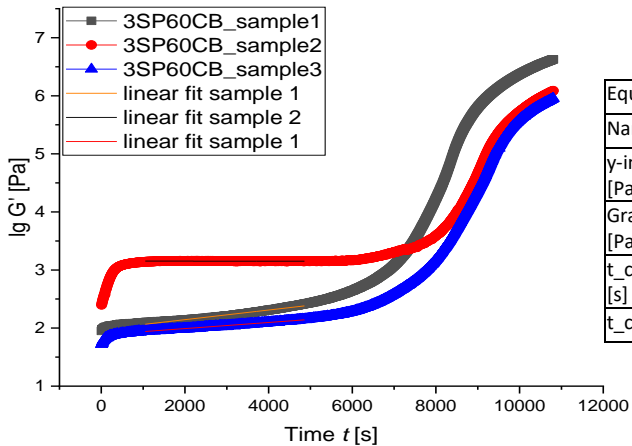
Equation	y = a + b*x		
Name	4SP60CB_sample1	4SP60CB_sample2	4SP60CB_sample3
y-intercept [Pa]	1.826 ± 0.001872	2.738 ± 2.454E-4	2.348 ± 3.83E-4
Gradient [Pa/s]	1.087E-4 ± 5.937E-7	4.525E-5 ± 7.786E-8	3.622E-5 ± 1.215E-7
t_cr_samplex [s]	5.9979E+03	6.4663E+03	6.5153E+03
t_cr [s]	6.3265E+03 ± 2.8559E+02		

Figure 54: Time-dependent measurement of emulsions, prepared with 4 wt% Soy protein. $lg G'$ is shown with linear fit to determine t_{cr} .



Equation	y = a + b*x		
Name	5SP60CB_sample1	5SP60CB_sample2	5SP60CB_sample3
y-intercept [Pa]	1.965 ± 0.002435	2.266 ± 4.213E-4	1.954 ± 0.001489
Gradient [Pa/s]	8.98E-5 ± 7.105E-7	8.637E-5 ± 1.23E-7	1.051E-4 ± 4.344E-7
t_cr_samplex [s]	5.9250E+03	6.6030E+03	6.2810E+03
t_cr [s]	6.293 ± 339		

Figure 53: Time-dependent measurement of emulsions, prepared with 5 wt% soy protein. $lg G'$ is shown with linear fit to determine t_{cr} .



Equation	y = a + b*x		
Name	3SP60CB_sample1	3SP60CB_sample2	3SP60CB_sample3
y-intercept [Pa]	1.979 ± 0.002024	3.153 ± 4.623E-4	1.886 ± 7.982E-4
Gradient [Pa/s]	8.294E-5 ± 6.419E-7	-1.79E-7 ± 1.467E-7	5.255E-5 ± 2.531E-7
t_cr_samplex [s]	5.7543E+03	6.9924E+03	6.1922E+03
t_cr [s]	6.3130E+03 ± 6.2779E+02		

Figure 52: Time-dependent measurement of emulsions, prepared with 3 wt% soy protein. $lg G'$ is shown with linear fit to determine t_{cr} .

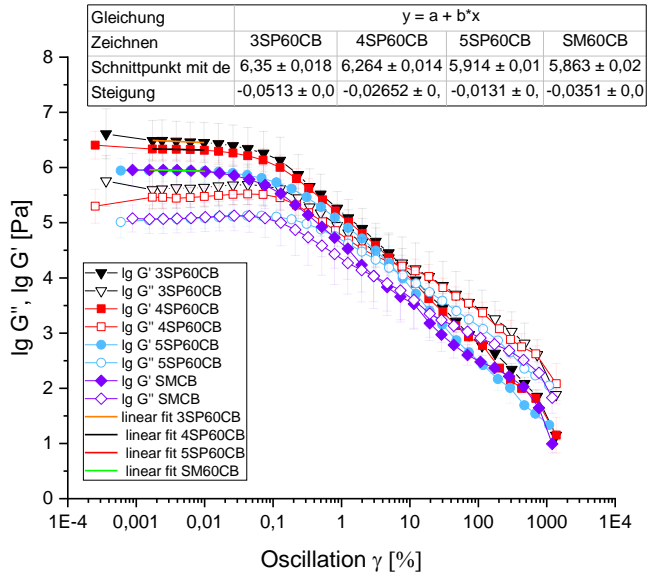


Figure 55: Amplitude-Sweep of emulsions, $\lg G'$ is shown with linear fit.

Acknowledgement

At this point I would like to thank all those who supported me during my bachelor thesis.

First of all, I would like to thank Prof. Dr. Thomas Vilgis from the Max Planck Institute of Polymer Research, who gave me my own small project and enabled me to write this bachelor thesis at the institute. Many thanks for the inspiring discussions and the support, whenever I had a question.

Also, many thanks to the Food Science Team at the Max Planck Institute of Polymer Research, who were always on my side with help and advice. I learned a lot from whom them.

My special thanks go to Andreas Hanewald without whom I would not have been able to perform my measurements during Corona.

Declaration of Originality

Bachelor's thesis in chemistry, biomedical chemistry or polymer chemistry
at the Johannes Gutenberg - University Mainz

I, Isabel Jungling, matriculation number 2738578

affirm that I wrote my bachelor thesis independently and did not use any other written and electronic sources or other aids than those indicated. All statements, that have been taken from other writings literally or analogously have been marked.

Mainz, 30.09.2020
(Place, date)

Isabel Jungling
(Signature)

Bachelorarbeit im Studiengang Chemie, Biomedizinische Chemie oder Polymerchemie an der Johannes-Gutenberg-Universität Mainz

Ich, Isabel Jungling, Matrikelnummer 2738578 versichere, dass ich meine Bachelorarbeit selbstständig verfasst und keine anderen als die angegebenen schriftlichen und elektronischen Quellen sowie andere Hilfsmittel benutzt habe. Alle Ausführungen, die anderen Schriften wörtlich oder sinngemäß entnommen wurden, habe ich kenntlich gemacht.

Mainz, 30.09.2020
(Ort, Datum)

Isabel Jungling
(Unterschrift)